LAWRENCE
LIVERMORE
NATIONAL
LABORATORY

LLNL-TR-820900

Neutron Induced Nuclear Reaction Cross Sections for Radiochemistry in the Region of Thallium, Lead, and Bismuth

R. D. Hoffman

March 26, 2021

Disclaimer

This work performed under the auspices of the U.S. Department of Energy by Lawrence Livermore National Laboratory under Contract DE-AC52-07NA27344.

LLNL-TR-820900

Neutron Induced Nuclear Reaction Cross Sections for Radiochemistry in the Region of Thallium, Lead, and Bismuth.

R.D. Hoffman
Nuclear Data and Theory Group
Physics and Life Sciences Directorate
Lawrence Livermore National Laboratory
Livermore, CA 94550
hoffman21@llnl.gov

March 26, 2021

ABSTRACT

We have developed a set of modeled nuclear reaction cross sections for use in radiochemical detector diagnostics. Systematics for the input parameters required by the Hauser-Feshbach statistical model developed in the TALYS code system are used to calculate neutron induced nuclear reaction cross sections for targets ranging from Thallium ($Z = 81$) to Bismuth ($Z = 83$).

Subject headings: Nuclear cross sections, Radiochemistry, Nuclear Physics

1. Introduction

1.1. Radiochemistry

Various aspects of nuclear explosive device performance can be determined through the application of radiochemical techniques. During the UGT (Under Ground Test) Program, select naturally occurring elements were often loaded into a device prior to a test and their activation products subsequently retrieved for counting. The radioactive products are reported as isotopic ratios (such as ^{87}Y/^{88}Y produced from a stable isotope of the naturally occurring element, in this case ^{89}Y). From the measured activity and prior knowledge of the amount of loaded detector material, performance aspects could be inferred by comparing the reported isotope ratios with those calculated using particle fluences from one of the design codes and group-averaged cross section sets that have been prepared for this purpose.

This study continues the collaborative effort between DP-Division(WCI) and NACS(PLS) to update, improve, and develop new cross section detector sets for radiochemical diagnostics.

Previous efforts treated the regions of:

- bromine and krypton (Hoffman *et al.* 2004a).
- iodine and xenon (Hoffman *et al.* 2004b).
- europium and gadolinium (Hoffman *et al.* 2004c).
- scandium, titanium, vanadium, chromium, manganese, and iron (Kelley *et al.* 2005).
- nickel, copper, and zinc (Kelley *et al.* 2006b).
- arsenic (Kelley *et al.* 2006a).
- yttrium, zirconium, niobium, and molybdenum (Hoffman *et al.* 2006c), (Hoffman *et al.* 2017).
- thulium, lutetium, and tantelum (Hoffman *et al.* 2015).
- iridium and gold (Hoffman *et al.* 2008).

Here we focus on cross sections in the region of thallium, lead, and bismuth.

Contents

List of Figures

List of Tables

1.2. Current Detector Sets

Over about 40 years (up to 1993) many cross section sets for radiochemical detector activation studies were developed at LLNL and LANL. At LLNL twenty-three neutron threshold detector sets and five charged particle sets were available at the end of the test program. The sets of interest in this modeling effort are as follows:

- Thallium neutron-induced set (never developed before now), used to calculate the production of the ground states of ^{200}Tl ($t_{1/2}$ = 26.1 h), ^{201}Tl ($t_{1/2}$ = 3.04 d), and ^{202}Tl ($t_{1/2}$ = 12.31 d) from stable ^{203,205}Tl.
- Bismuth neutron-induced set (Bi0389), used to calculate the production of ^{205}Bi ($t_{1/2}$ = 15.31 d), ^{206}Bi ($t_{1/2}$ = 6.24 d), ^{207}Bi ($t_{1/2}$ = 31.55 y), and ^{208}Bi ($t_{1/2} = 3.68 \times 10^5$ y) from stable ^{209}Bi. Note that the decay half-life for ^{207}Bi has decreased (by 2%) from its previous value cited in (Nethaway 1998).

The cross sections available in the Bismuth detector set are summarized in Table 2 in appendix A. The bismuth set includes (n,γ) (n,2n), and (n,3n) cross sections on ground states. Our new thallium set will include the same cross sections and both sets will also be calculated on ground state targets only. We also develop these same cross sections for stable isotopes of lead to discern the ability of the TALYS code system to accurately calculate measured cross sections in this region of interest.

1.3. Motivation for Updating the Detector Sets

Many of the historical RADCHEM detector sets updated in our previous modeling efforts had a clear need for improvement. Several of the historical cross section sets did not include charged particles in the exit channel of the neutron-induced reactions. Here, because these targets have such a high Z value, charged particles are strongly inhibited by the Coulomb barrier in the exit channel, so the dominant reactions will only involve neutrons and photons.

Another motivation is drawn from the general improvement in cross section modeling capabilities. In the nearly three decades since the historical sets were developed, many new cross section measurements have been performed, and the amount of nuclear structure data used to constrain model parameters has improved. Additionally, several efforts have been made to develop consistent approaches to modeling nuclear reaction cross sections (Belgya *et al.* 2005), and there are more accurate methods of calculating and estimating cross sections for which we have no data.

Lastly, here (and in our previous efforts) we include an in-depth investigation into the sensitivity of the modeled cross sections to variations in the many statistical model inputs, enabling us to determine which parameters are the most important for a given reaction. This allows us to estimate how much a calculated cross section will change if new experimental measurements place more constraints on the model inputs, and to calculate upper and lower bounds to our central value cross sections for use in UQ studies.

1.4. Proposed Detector Sets

We consider as targets the ground states of the isotopes listed in Table 2 of Appendix A. For each of these targets, we model the reaction channels indicated in the table. This modeling effort includes all of the reactions previously available in the RADCHEM Bismuth detector set, but also reaction channels included primarily to provide further comparisons to measured cross section data and bolster our confidence in the accuracy of cross sections modeled for unstable targets.

Our goal is to develop a consistent set that reproduces, as closely as possible, measured cross sections on targets in the *local region of interest*. To do this we modify the *global systematics* developed in the TALYS code system for the many input quantities used in the theoretical reaction modeling calculations. Systematics are based on experimental data that are often only available for compound nuclear systems formed from a stable target plus a neutron. Of course, we use experimental data whenever it is available, but reactions proceeding through unstable systems are unavoidable in radiochemistry. Short of developing new experimental techniques to measure cross sections on unstable targets, our only hope of reproducing measured activity from UGT shots, and addressing the uncertainty associated with the nuclear cross sections, is to develop cross section sets that reproduce well the measured cross sections in the local region of interest.

In §2 we describe the theoretical techniques used in the modeling effort. §3 describes the input parameters. §4 gives results. We conclude with §5.

2. Nuclear Reaction Theory

2.1. Reaction Mechanisms

Conceptually, we consider nuclear reaction mechanisms to be of two general types: direct processes and compound processes. Direct processes can be pictured as simple interactions of the incident particle with the nuclear potential of the target nucleus. They proceed on a rapid time scale (of order $\sim 10^{-22}$ s), and the reaction products are often highly peaked in the incident particle direction.

Compound processes are pictured as complicated interactions proceeding over a much longer timescale ($10^{-15} - 10^{-18}$ s) in which the reaction is mediated by the formation of a "compound nucleus", with the excitation energy of the incident particle being statistically "shared" with the ensemble of nucleons in the target over all energetically allowed degrees of freedom. The reaction products are largely isotropic.

Other intermediate reaction mechanisms exist between these two extremes. We refer to these as "pre-equilibrium" nuclear processes, where a particle may be emitted from the target+projectile compound system prior to equilibration. Over the energy range of interest to this project (a few keV to 20 MeV) all of these processes will be included in our cross section calulations with the pre-equilibrium and compound nuclear processes proving to be most important.

2.2. Hauser-Feshbach Statistical Model

A traditional theoretical approach to compound nuclear reactions is the statistical or Hauser-Feshbach model (Hauser & Feshbach 1952). This model is valid for high level densities in the compound nucleus, allowing one to use energy averaged transmission coefficients T, which describe absorption via an imaginary part in the nucleon-nucleus potential (Mahaux & Weidenmüller 1979). For the reaction I (in state μ) $+j \rightarrow k +$ L (in state ν), with I$^\mu$ + j interacting with center-of-mass energy E$_j^\mu$ (in MeV), the average cross section is given by

$$\sigma_{jk}^{\mu\nu}(E_j^\mu) = \frac{\pi\lambda\!\!\!^{-2}_j}{g_I^\mu g_j} \sum_{J,\pi} g_J \frac{T_j^\mu(J^\pi) T_k^\nu(J^\pi)}{T_{tot}(J^\pi)} W(J^\pi) \tag{1}$$

where the summation extends over all compound nuclear spins and parities J^π, μ and ν enumerate states in the target and product (=0 for the ground state, 1 for the 1^{st} excited state, etc.). The cross section has units of area, described by $\pi\lambda\!\!\!^{-2}_j = 0.6566(\hat{A}_j E_j^\mu)^{-1}$ barns, with $\hat{A}_j = (A_I A_j)/(A_I + A_j)$ being the reduced mass in atomic mass units and E_j^μ is the center of mass energy in units of MeV. $\lambda\!\!\!^{-}_j$ is the wavelength related to the wave number k_j in the target plus incident particle channel by $\lambda\!\!\!^{-}_j = 1/k_j$ The statistical weights are given by $g_y^x = (2J_y^x + 1)$. Items without superscripts refer to the compound nucleus.

The transmission coefficients in the numerator are given by $T_j^\mu(J^\pi)$ = the total transmission coefficient for forming the state J^π in the compound nucleus $I^\mu + j$ at energy E_j^μ. Likewise, $T_k^\nu(J^\pi)$ is the same as $T_j^\mu(J^\pi)$ but for the pair $L^\nu + k$ at energy E_k^ν. Implicit in these definitions is a sum over all possible $l-$waves and channel spins, i.e.

$$T_j^\mu(J^\pi) = \sum_{l,s} T_j^\mu(J^\pi, l, s) \tag{2}$$

where l is any partial wave number (orbital angular momentum) that can couple the state μ to the compound nuclear state having spin and parity J^π subject to quantum mechanical selection rules and s is the vector sum of the spins J_I^μ and J_j. Hence s takes on all integer (or half-integer) numbers from $|J_I^\mu - J_j|$ to $J_I^\mu + J_j$.

T_{tot} represents the sum of transmission coefficients over all possible decay channels (i.e. for all particles and photons). The cross section for the formation of species L, regardless of its state ν, is obtained by summing Eq. [1] over all bound states ν of L for which the reaction is energetically allowed.

When evaluating these sums, if energies become of interest which exceed the highest discrete excited state for which energy, spin, and parity are explicitly known, a nuclear level density formula must be employed. Specifically, the definitions for the transmission coefficients $T_j(J^\pi)$, $T_k(J^\pi)$, and $T_{tot}(J^\pi)$ must be modified:

$$T_k(J^\pi) = \sum_{\nu=0}^{\omega} T_k^\nu(J^\pi) + \sum_{J^\nu \pi^\nu} \int_{\xi_L^\omega}^{\xi_L^{max}} T_k^\nu(\xi_L^\nu, J^\pi) \rho(\xi_L^\nu, J^\nu, \pi^\nu) d\xi_L^\nu d\pi^\nu dJ^\nu \tag{3}$$

where for the nucleus L, ξ_L^ω is the energy of the highest excited state, ω, of known energy, spin, and parity; $\xi_L^{max} = E_k^0 = E_j^0 + Q_{jk}$ is the maximum excitation energy available, and $\rho(\xi_L^\nu, J^\nu, \pi^\nu)$

is the density of states per unit energy of spin and parity J^ν and π^ν at the excitation energy ξ_L^ν. The above integral approximates a sum and is subject to the same quantum mechanical restrictions implied in the definition of the transmission function.

2.3. Width Fluctuations

In addition to the ingredients required for Eq. [1], we apply width fluctuation corrections ($W(J^\pi)$, hereafter WFC), which define correlation factors with which all partial channels of incoming particle j and outgoing particle k, passing through excited state (E, J, π), should be multiplied. The major effect is to enhance the elastic channel and accordingly decrease the other open channels. They are most often observed at or near channel opening energies, for example when a (p,γ) and a (p,n) channel compete and the weaker (p,γ) channel is enhanced. Above a few MeV of excitation energy, when many competing channels are open, WFC's can be neglected. For our purposes they only affect the neutron capture cross sections.

A reasonably complete treatment for the WFC, obtained with the Gaussian orthogonal ensemble (GOE) approach, requires the evaluation of a triple integral and to date has been considered much to costly to apply in nuclear cross section calculations. Two popular approximations are from (Hofmann *et al.* 1975) and (Moldauer 1976) (the TALYS default).

2.4. Pre-Equilibrium Processes

When comparing statistical model cross sections to experimentally determined ones it is well known that the contributions due to pure compound processes are too small at excitation energies starting around 10 MeV, whereas direct processes only excite the discrete levels at the highest outgoing energies. Between these two ranges an intermediate process with aspects of both appears to be needed, pre-equilibrium.

We adopt the default exciton model in TALYS (described in Sec 4.4.1 of the TALYS manual) which has an initial 2-particle 1-hole configuration. In this model the nuclear state is characterized by a total energy and the total number of particles above and holes below the Fermi surface. The exciton model is a time-dependent master equation which describes the probability of transitions to complex particle-hole states and to the continuum. Integration over time results in an energy-averaged emmission spectrum.

In the the pre-equilibrium stage of the reaction, particle emission is assumed to be the only decay mode and is applied only to the cross section resulting from the formation of the compound nucleus. For our purposes there is one adjustable free parameter, **M2constant**, that will be used to determine the amount of pre-equilibrium applied.

2.5. The TALYS Hauser-Feshbach Reaction Code

We model our cross sections using the statistical model code TALYS-1.8 (28), which embodies all of the physical models discussed above. A prior version of the code (1.4) was used to develop the RADCHEM cross section sets for Thulium, Lutetium, and Tantelum (Hoffman *et al.* 2015).

3. Inputs to the Hauser-Feshbach Model

Here we discuss the important ingredients of statistical model calculations, and the methods utilized to estimate them. These include the requisite nuclear structure data, such as the binding energies of all nuclei included (which define the separation and reaction threshold energies and Q-values of the various reaction channels considered), as well as the energies, spins, and parities of the ground states and all known excited states of these nuclei, and the detailed branching ratios for the gamma-ray cascade from excited to low-lying states. Also needed are parameters controlling the width fluctuation corrections and the pre-equilibrium model, the particle and γ-transmission coefficients, and the nuclear level densities of all nuclei involved in a given reaction. The reliability with which these ingredients can be calculated (or estimated based on fits to experimental data) determines the accuracy (or reliability) of a given cross section calculation.

Some of these input quantities can be constrained by experimental data derived from resonance studies on compound nuclear systems starting on stable nuclei. For other nuclei systematics are needed. These are typically developed as fits to the resonance results over a local or global range of the periodic chart. We will illustrate the systematics developed in the TALYS code for various input quantities and show how well the default systematics produce cross sections for which experimental data is available.

The default TALYS input file for ^{209}Bi + n and the default choices for various models and parameters are given in Appendix A.3.

3.1. Nuclear Structure Data

3.1.1. Nuclear Masses, Q-values

The TALYS input keywords **expmass** and **massmodel** determine what database nuclear mass excesses are drawn from. Default values are "**yes**" and "**2**", so that experimental mass excess values (Wapstra *et al.* 2003; Audi *et al.* 2003) are used. In Appendix A.2 we provide reaction Q-values calculated from the experimental masses for all cross sections modeled in this study.

3.1.2. Nuclear Level Schemes

The nuclear level schemes for the all species are based on the discrete level file of Beglya (RIPL-2 database) and are located in the "levels" subdirectory in the TALYS structure database. Three options are available depending on the input to TALYS keyword "**disctable**", the default vaule is "**1**". Important quantities drawn from these tables are level energies, spin and parity assignments, and gamma-decay branching ratios.

3.2. Transmission Coefficients

3.2.1. Transmission Coefficients for Particles

Energy-averaged transmission coefficients are needed for each particle considered as a possible exit channel in the Hauser-Feshbach denominator. By default TALYS uses neutrons, protons, deuterons, tritons, and alpha particles in the development of the transmission coefficients. Due to the very large coulomb barriers associated with these heavy targets, we found that all neutron-induced reactions with charged particles in the exit channel were very small. We therefore focus the following discussion on the neutron optical potential only, and chose as input to the TALYS keyword "**ejectiles**" both "**g**" and "**n**", which limited cross section output to neutron-induced reactions only.

3.2.2. Considerations Regarding Collectivity and Nuclear Deformations

Our region of interest extends from Tl to Bi over the neutron number range $118 \leq N \leq 126$. To gauge the onset of collective effects we appeal to nuclear systematics. One such measure of "collectivity" is the ratio vs. neutron number N of the energy of the first $J^\pi = 4^+$ excited state to the first $J^\pi = 2^+$ excited state in even-Z even-N nuclei (Figure 1). Spherical (magic closed shell) nuclei exhibit collectivity near 1.6 and are clearly

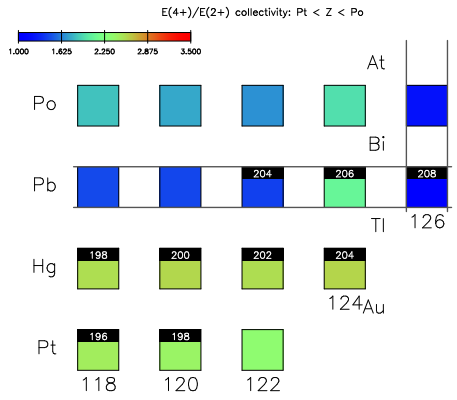

Fig. 1.— Collectivity (the ratio of energies of the first 4+ and 2+ levels in even-Z even-N nuclei) in the region from Platinum to Polonium. The scale gives the ratio E(4+)/E(2+), 1.0 (blue) is spherical, 2.3 (green) transitional, and ≥ 3 (red) is strongly deformed.

seen in the Z=82 (Pb) closed proton shell. Deformed vibrators occur between 2.0 - 2.4 (Pt and Hg with $118 \leq N \leq 124$). True rotational nuclei, characterized by deformation ratios up to 3.3, are not evident in this region of interest. The loaded radchem species ^{203,205}Tl, and ^{209}Bi sit firmly in a zone of fairly weak deformation.

3.2.3. The Neutron Optical Potential

By default TALYS adopts the optical model of (Koning & Delaroche 2003) for calculation of particle transmission coefficient (see Section 4.1 of the TALYS use manual). Although Koning et al. tuned their parameters to fit data for many different species (see their Tables 6 and 7), TALYS uses the global nucleon-nucleon optical model potential (OMP), as it gives a fairly satisfactory fit to measured total neutron cross section data in the range of interest to us. Specifically, TALYS adopts the potential depth parameters and Fermi energies for the neutron and proton global OMP defined in Koning's Section 5.2, tables 14 and 15. TALYS generates particle transmission coefficients using the built-in optical model code ECIS-96 (Raynal 1996). Although designed for coupled channel calculations, TALYS defaults to using the code in a spherical optical model mode. For Tl and Bi targets this is the only mode possible, as neither of these elements has an entry in the *TALYS/structure/deformation/* database.

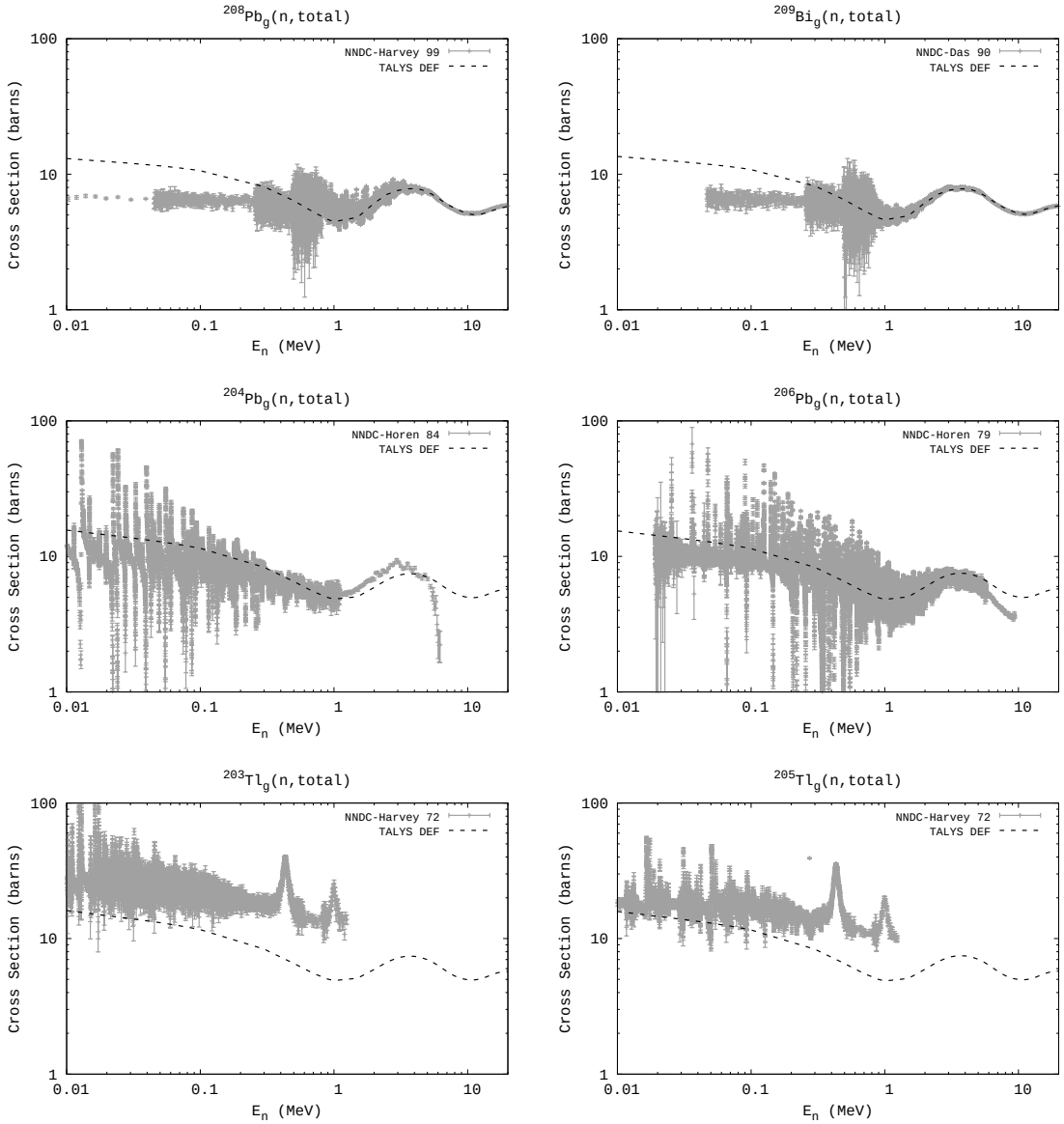

Fig. 2.— Measured total neutron cross sections vs. those predicted by the optical model of Koning-Delaroche for select stable targets in the range $81 \leq Z \leq 83$. Measured data were obtained from the EXFOR database (NNDC 2006). The optical model prediction is indicated by the dashed black line.

3.2.4. Evaluation of the Neutron Optical Potential

In Figure 2 we show measured vs. calculated total neutron cross sections for select stable targets between Tl and Bi. Good agreement is seen for Bi and Pb targets, but the Tl targets are calculated low (by nearly a factor of two) compared to measured cross sections. We note that all these calculated total neutron cross sections are very nearly identical.

At lower energies, the measured total neutron cross sections generally exhibit structure due to individual resonances. This structure cannot be reproduced by an optical model, which only predicts average cross sections.

3.2.5. Transmission Coefficients for Photons

Gamma-ray transmission coefficients (described in section 4.3 of the TALYS user manual) are based on a simple model that depends only on the multi-pole type (X = M or E for magnetic or electric) and the transition energy (E_γ). They

are related to the gamma ray strength function $f_{Xl}(E_\gamma)$ by

$$T_{Xl}(E_\gamma) = 2\pi f_{Xl}(E_\gamma) E_\gamma^{2l+1} \quad (4)$$

The energy dependence of the strength function is determined using a Giant Dipole resonance (GDR) model. By default TALYS (input parameter **strength 1**) uses a simple Brink-Axel option for all transitions that are not E1, with a standardized Lorentzian form that describes the giant dipole resonance shape

$$f_{Xl}(E_\gamma) = K_{Xl} \frac{\sigma_{Xl} E_\gamma \Gamma_{Xl}^2}{(E_\gamma^2 - E_{Xl}^2)^2 + E_\gamma^2 \Gamma_{Xl}^2} \quad (5)$$

where E_{Xl}, Γ_{Xl}, and σ_{Xl} are GDR resonance parameters for the energy, width, and strength of the giant resonance, and

$$K_{Xl} = \frac{1}{(2l+1)\pi^2 h^2 c^2}. \quad (6)$$

For E1 transitions TALYS uses a generalized Lorentzian form from Kopecky and Uhl (Kopecky *et al.* 1993):

$$f_{E1}(E_\gamma) = K_{E1} \times \left[\frac{E_\gamma \tilde{\Gamma}_{E1}(E_\gamma)}{(E_\gamma^2 - E_{E1}^2)^2 + (E_\gamma^2 \tilde{\Gamma}_{E1}(E_\gamma)^2} + 0.7 \frac{\tilde{\Gamma}_{E1} 4\pi^2 T^2}{E_{E1}^3} \right] \quad (7)$$

where the energy dependent damping width $\tilde{\Gamma}_{E1}$ is given by

$$\tilde{\Gamma}_{E1}(E_\gamma) = \Gamma_{E1} \frac{E_\gamma^2 + 4\pi^2 T^2}{E_{E1}^2} \quad (8)$$

and the nuclear temperature T is gien by

$$T = \sqrt{\frac{E_n + S_n - \Delta - E_\gamma}{a(S_n)}} \quad (9)$$

Experimental GDR resonance parameters for the first resonance are available in this region (Belgya *et al.* 2005), otherwise systematics for E1, M1, E2, and M2 transitions are used (see equations 4.72-4.76 in the TALYS user manual and figures 4 - 5). Over the range of nuclei shown few quantities show large variations, and most can be treated as constants.

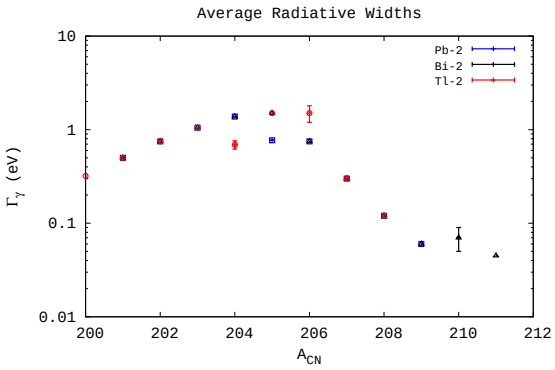

Fig. 3.— Average radiative widths from Experiment (RIPL-2) and systematics (Kopecky).

3.2.6. Normalization of γ-ray Strength Functions

The gamma-ray strength function is normalized using the value of the average radiative width (Γ_γ) at the neutron speration energy (S_n). TALYS uses experimentally derived values of Γ_γ where available, and an interpolation formula from Kopecky for $40 \leq A \leq 250$ when they are not. At low incident neutron energies Γ_γ is due almost entirely to the s-wave interaction. $\Gamma_\gamma(S_n)$ can be calculated by integrating the γ-ray transmission coefficients over the density of final states reached in the first step of the γ-ray cascade through the use of a normalization constant G_{norm} as given by Eq. (4.79) in the TALYS user manual.

Figure 3 shows default Γ_γ values. A single systematic for isotopes of all three elements is fit to the experimental data. The average uncertainty on each data point is roughly 20-30 percent. If $G_{norm} = 1$ is specified no normalization is carried out and strength functions are calculated using only the GDR parameters previously discussed.

3.3. Nuclear Level Densities

3.3.1. Level Density Models

Another necessary input to the statistical model code is the nuclear level density. TALYS has five models available. By default (input parameter **ldmodel 1**) TALYS adopts a standardized, semi-empirical approach (the Constant Temperature Model) which is numerically efficient, can be tied to experimental data, and is fairly accurate (Gilbert & Cameron 1965). The level density is described by two functions. Both are energy dependent, the second factor contains the spin dependence:

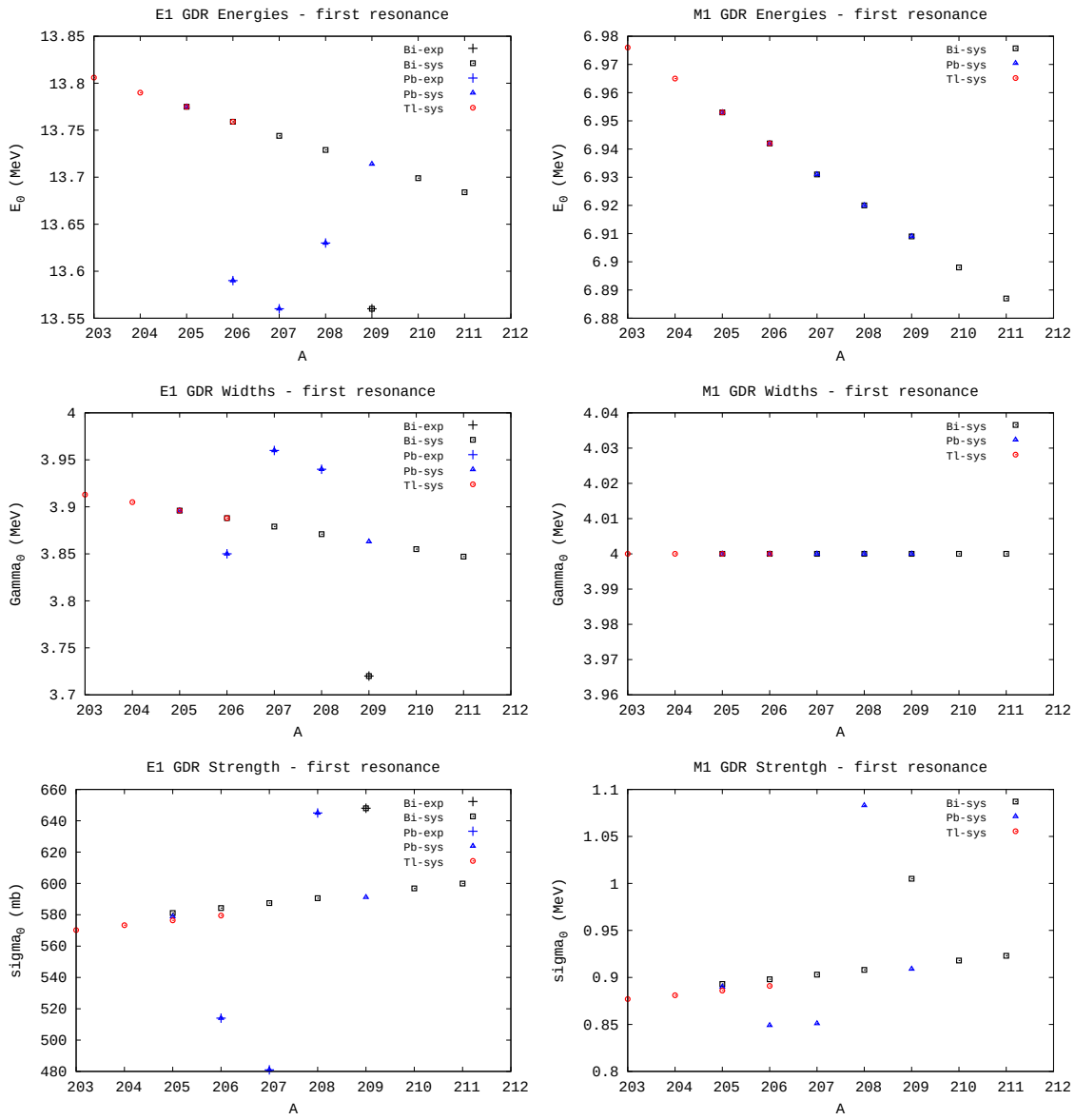

Fig. 4.— Giant dipole resonance parameters (1^{st} resonance): GDR energy(top), width(middle), and strength(bottom) are shown for E1(left panels) and M1(right panels) transitions. Each value is color coded for Tl(red), Pb(blue), and Bi(black) targets in our region of interest. Both experimental ("+") and systematic values are shown.

$$\rho\left(U,J\right)=\rho\left(U\right)f\left(U,J\right) \tag{10}$$

where $\rho(U)$ is the state density, with $U=E-\Delta$ the back-shifted energy. Δ is the so called "pairing energy", and J is the spin of the compound nucleus. For the state density we assume a Fermi gas formula:

$$\rho\left(U\right)=\frac{\sqrt{\pi}}{12}\,\frac{\exp\left(2\sqrt{aU}\right)}{a^{1/4}U^{5/4}}\,\frac{1}{\sqrt{2\pi}\sigma} \tag{11}$$

$$f\left(U,J\right)=\frac{2J+1}{2\sigma^{2}}\,\exp\left[\frac{-\left(J+\frac{1}{2}\right)^{2}}{2\sigma^{2}}\right] \tag{12}$$

where $a(U)$ is the level density parameter (in MeV^{-1}). The spin cutoff parameter σ^2 characterizes the spin distribution of the Fermi gas level density and has various forms in different energy ranges, see below. This level density formulation assumes an equal distribution of parity states. Note that at low excitation energy (for a positive back-shift), Eq. 11 diverges.

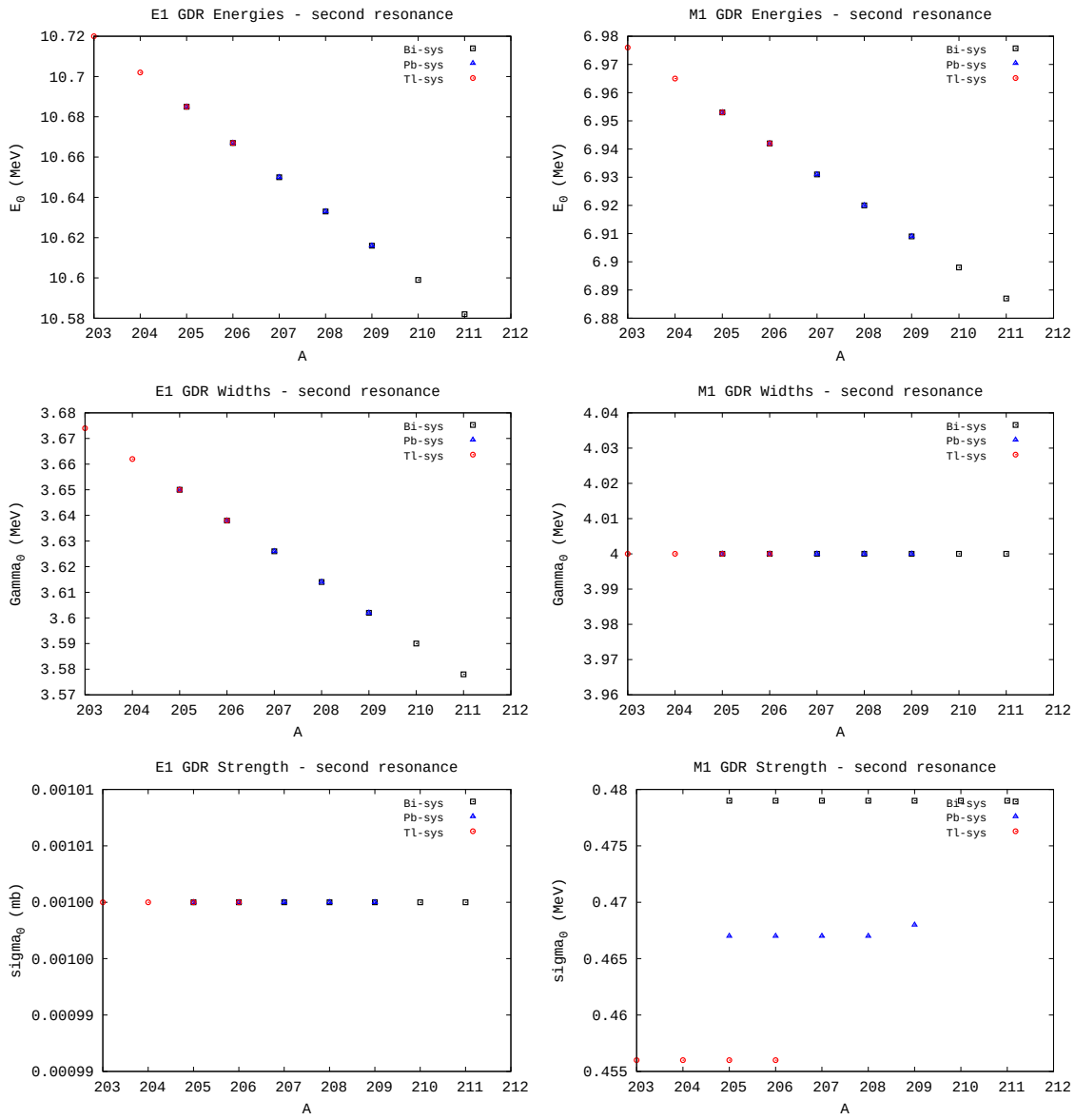

Fig. 5.— Giant dipole resonance parameters (2^{nd} resonance): GDR energy(top), width(middle), and strength(bottom) are shown for E1(left panels) and M1(right panels) transitions. Each value is color coded for Tl(red), Pb(blue), and Bi(black) targets in our region of interest. Only systematic values are shown.

In the Fermi-gas state density (Eq. 11) the level density parameter $a(U)$ can be related to the average level spacing (D_0) near the neutron binding energy. For a target with zero spin:

$$D_{calc} = \frac{2}{\rho\left(U, J = \frac{1}{2}\right)} \tag{13}$$

while for non-zero spin targets:

$$D_{calc} = \frac{2}{\rho\left(U, J = s + \frac{1}{2}\right) + \rho\left(U, J = s - \frac{1}{2}\right)} \tag{14}$$

Figure 6 shows average level spacings used by default in TALYS. There are three seperate systematics with an odd-even staggering, each apparently fit to the measured D_0 values for the given element. All are rising, indicating smaller level densities as one approaches the N=126 closed shell. Also shown are the level density parameters that correspond to these level spacings.

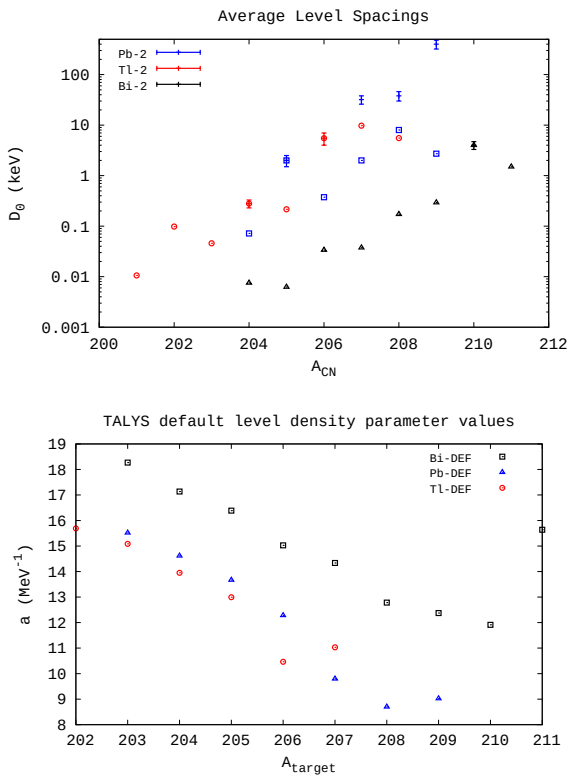

Fig. 6.— Average level spacings, D_0, and corresponding level density parameters $a(U)$.

3.3.2. *Level Densities Above the Neutron Binding Energy*

By default TALYS adopts an energy dependent form for the level density parameter, $a(U, Z, N)$, (Iljinov *et al.* 1992), that depends on the spin cutoff parameter σ^2 and the pairing energies Δ.

3.3.3. *The Spin Cutoff Parameter*

TALYS uses various forms for the spin cutoff parameter σ^2 depending on the location of the matching energy E_x. It is defined by relations given by equations (4.251) - (4.257) in the TALYS user manual.

3.3.4. *Pairing Energies*

The back-shift Δ, also known as the pairing energy, is given a simple form in the Constant Temperature model: $\Delta(Z, N) = 12\chi/\sqrt{A}$, where $\chi = 0$ for odd-odd, 1 for odd-even, and 2 for even-even nuclei.

3.3.5. *The Level Density Parameter*

By default TALYS assumes an energy dependent level density parameter ((Iljinov *et al.* 1992))

$$a(U) = \tilde{a}\left[1 + \delta W \frac{f(U)}{U}\right] \tag{15}$$

with $f(U) = 1 - \exp(-\gamma U)$. The asymptotic level density parameter $\tilde{a}$ is of the form $\tilde{a} = \alpha A + \beta A^{2/3}$. For the constant temperature model $\alpha = 0.06926$, $\beta = 0.28277$, and $\gamma = \gamma_1/A^{1/3}$ with $\gamma_1 = 0.43309$. The shell corrections δW are differences between experimental and theory masses based on the spherical droplet model of Meyers & Swiatecki. See equations (4.244) - (4.245) in the TALYS user manual. For default $a(U)$ values see Figure 6.

3.3.6. *Level Densities Below the Neutron Binding Energy*

At and below the pairing energy Δ, the state density in Eq. 11 becomes imaginary. By default TALYS uses a constant temperature formula for the state density

$$\rho(E) \propto \exp\frac{E - E_0}{T} \tag{16}$$

The constant temperature parameters E_0 and T, can be chosen to provide a state density that goes through the low lying spectroscopic levels subject to a matching energy, E_x, chosen someplace between the high and low energy regions of interest, at which the two state densities match (point and slope).

A clear strength of the TALYS code is that it chooses values for all the level density parameters using experimental data (where available) or systematics derived from them and performs the low temperature fits automatically. Of course the user has full control over all paramaters, but this serves as a useful first step in any evaluation. See Appendix A.4 for default level density parameters calculated by TALYS using the models and data mentioned above.

This concludes our presentation of inputs that are constrained by experimental data and the TALYS systematics for those inputs. We next present experimentally measured cross sections for various channels on Tl, Pb, and Bi targets and illustrate how well a default TALYS calculation agrees with experiment. We also suggest modifiactions to the TALYS input file that brings the default calulations into better agreement with the measured cross sections and their uncertainties.

4. Modeled Cross Section Results

4.1. Tl & Bi (n,2n) cross sections: TALYS vs. experiment

Above their reaction threshold energies (n,2n) cross sections depend on target spins and the treatments of the optical model (used to calculate the particle transmission coefficients), the nuclear level density, and pre-equilibrium (Eq. 1). Especially important is the neutron transmission coefficient, since in an (n,2n) calculation it appears in both the entrance and exit channel of the numerator. Since these heavy targets have large coulomb barriers, the charged-particle transmission coefficients in the hauser-feshbach denominator will be small, and the neutron transmission coefficent in the sum will be canceled by one in the numerator, leaving only the factors mentioned above to determine the (n,2n) cross section. The gamma-ray transmission coefficient plays little role (since γ-widths are nearly always smaller than particle widths).

The optical model has been highly optimized using a large number of parameters, Figure 2 shows how well the measured total neutron cross sections agree with experiment.

The level densities are tied to experimental data through the average level spacings. Figure 6 shows the thallium and lead systematics apparently fit to the two measured D_0 values, while bismuth only has one value to anchor its systematic. All three are rising, indicating smaller level densities as one moves towards higher mass numbers. The bismuth systematic is the smallest, hence the level density parameters returned will be the largest of the three. They also appear to exhibit an odd-even staggering. Whatever motivation was used to develop these systematics, they do go through the available data.

The pre-equilibrium treatment in TALYS can be adjusted with a scaling parameter **M2constant** that serves as a multiplier on the imaginary potential well depth of the neutron optical model (see section D2 in chapter 4 of the TALYS user manual).

Calculated vs. experimental (n,2n) cross sections for stable targets of Tl and Bi are presented in Figure 7 (for Pb targets see Appendix B.1). The ^{209}Bi(n,γ)^{210}Bi cross section from Bi0389 is shown as the brown dashed line. The dashed black line is the default TALYS calculation (**M2constant=1.0**). Clearly TALYS overpredicts the two thallium (n,2n) cross sections

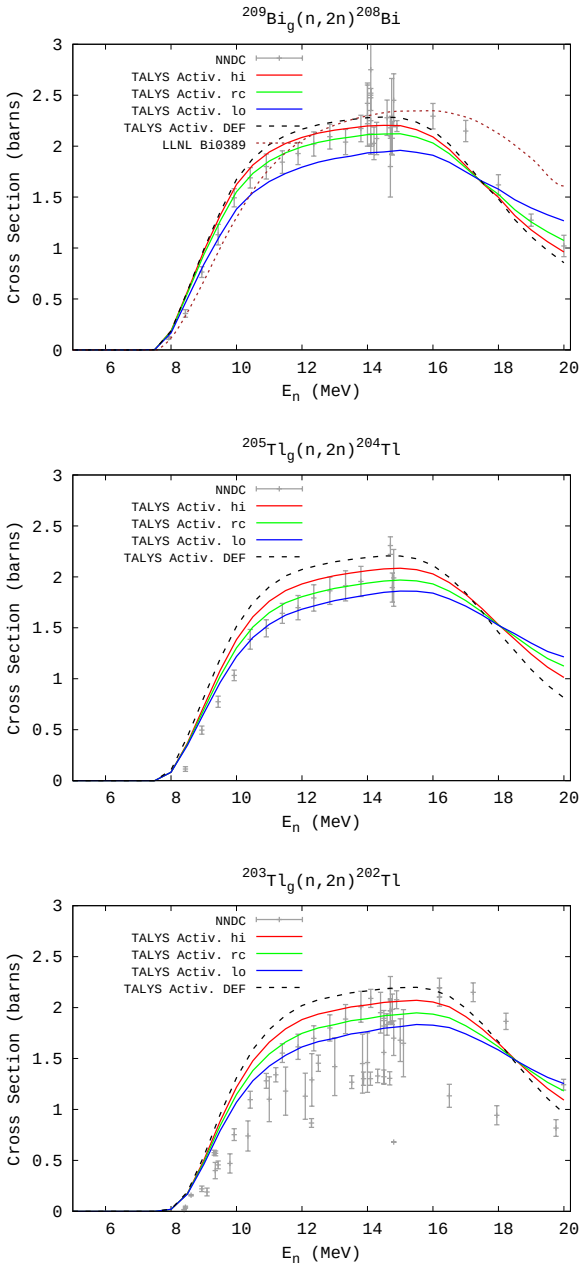

Fig. 7.— Calculated vs. measured (n,2n) cross sections on the stable isotopes of Tl and Bi. Experiemntal data is taken from (NNDC 2006). The LLNL Bi0389 cross section is shown as the brown dashed line. The dashed black line is the TALYS default calculation. The green, red, and blue lines represent our recommended cross section and its upper and lower bound.

which is puzzling since the optical model underpredicts their total neutron cross sections (Figure 2). It should be noted all three TALYS default

(n,2n) calculations peak near 15 MeV at $\sim$ 2.2 barns, suggesting an optical model that shows very little variation across this region.

To bring the default calculations into line with experiment the pre-equilibrium scaling parameter **M2constant** was adjusted, leaving the level density and optical model treatments untouched. This choice has advantages, in that pre-equilibrium effects only appear above a few MeV of incident neutron energy, and will not affect the neutron capture cross sections which are small (and getting smaller) as the pre-equilibrium effects become apparent. The green line represents our recommended (n,2n) cross section, the blue and red lines its lower and upper bounds, respectively. The amount of scaling was chosen to span the range of uncertainty in the measured (n,2n) cross sections and was uniformly applied to all targets for a given element. For Bi we used M2constant = 0.2, 0.4, and 0.6 to calculate the lower bound, recommended, and upper bound cross sections respectively (we applied the same scaling to the Pb targets). For Tl we used 0.2, 0.3, and 0.5. At 14 MeV these choices lead to (n,2n) cross sections that are on average +5% and -7% above and below our recommended cross sections for all targets considered in this study.

We note that had we chosen to adopt only the M2constant scaling needed to produce our recommended cross section, the variation in level density provided by the uncertainty in the measured average level spacings would be insufficient to span the range of experimental uncertainty seen in the measured cross sections.

4.2. Tl & Bi (n,3n) cross sections: TALYS vs. experiment

The (n,3n) cross sections are determined by the same quantities as the (n,2n) cross sections. Therefore we have again scaled our default calculations with the **M2constant** parameter to bring our default (n,3n) cross sections in agreement with experiment. Figure 8 shows our calculated TALYS (n,3n) cross sections on Tl and Bi targets vs. experimental data where available (for Pb targets see Appendix B.2). The thresholds for these cross sections are above 14 MeV in all cases in this mass range, reflecting the rapid fall off of the (n,2n) reaction channel. The scaling chosen for the Pb and Bi isotopes was again 0.2, 0.4, and 0.6, while for Tl it was 0.3, 0.5, and 1.0 for our lower, recommended, and upper bound (n,3n) cross sections, respectively.

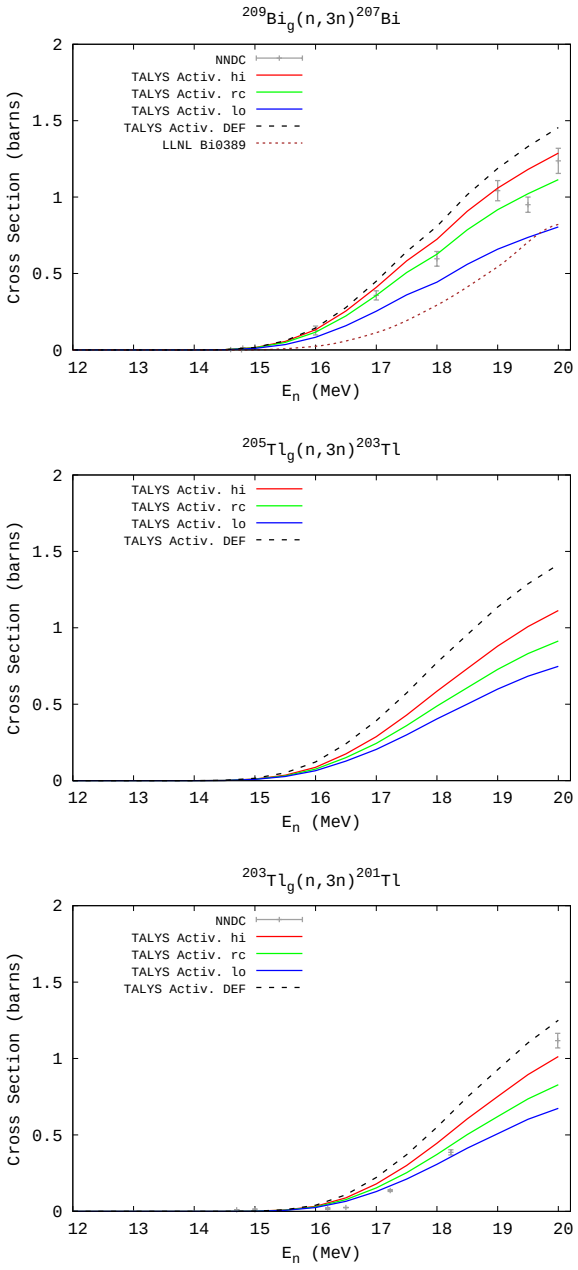

Fig. 8.— Calculated vs. measured (n,3n) cross sections on the stable isotopes of Tl and Bi. Experimental data is taken from (NNDC 2006). The LLNL Bi0389 cross section is shown as the brown dashed line. The dashed black line is the TALYS default calculation. The green, red, and blue lines represent our lower bound, recommended, and upper and lower bound (n,3n) cross sections.

4.3. Tl & Bi (n,γ) cross sections: TALYS vs. experiment

For keV energies neutron capture cross sections depend only on target spins and the treatments of

the nuclear level density and the gamma-ray transmission coefficients (Eq. 1). This is so because charged particle cross sections for heavy targets always have thresholds of a few MeV. For energies below that their transmission coefficients will be small, making the neutron transmission coefficient the dominant term in the hauser-feshbach denominator. This cancels the same term in the numerator, leaving only the factors mentioned above to determine the capture cross section.

The level densities and gamma-ray transmission coefficients are tied to experimental data through the average level spacing D_0 and the average radiative widths Γ_γ, respectively (see figures 3 and 6). Ideally, calcuated capture cross sections on stable targets with measured values for both of these quantities should agree with experimentally measured ones provided the treatments of the level density and the gamma-ray strength functions are reasonable approximations.

In our region of interest only ^{203,205}Tl, ^{204}Pb, and ^{209}Bi all have measured average level spacings and radiative widths with uncertainties that are used in the default TALYS calculation. But even in this scenario "best case" scenario we see that with one exception (^{205}Tl) the agreement with experiment is only good to within a factor of two.

Since experimental data on capture cross sections (NNDC 2006) is sparse in this mass range we compare our calculations to the evaluated capture cross sections from the KADONIS group (Bao *et al.* 2000). The Maxwellian-averaged neutron capture cross section (MACS) is defined as the reaction rate $\langle \sigma v \rangle$ divided by the mean velocity $v_T = \sqrt{2kT/\mu}$ at a given temperature T. Here, μ is the reduced mass. For particle fluences and temperatures typical to stellar nucleosynthesis, the velocity distribution of the neutrons is well described by a Maxwell-Boltzmann distribution. In this case, the Maxwellian-averaged cross section reduces to (Beer *et al.* 1992)

$$\frac{\langle \sigma v \rangle}{v_T} = \frac{\int_0^\infty \sigma_{n\gamma} v \Phi(v) dv}{v_T} = \frac{2}{\sqrt{\pi}(kT)^2} \int_0^\infty \sigma_{n\gamma}(E) W(E, kT) dE \quad (17)$$

where $W(E, kT) = E \exp(-E/kT)$ and E is the center of mass energy.

Table 1 shows the MACS from KADONIS vs. our default TALYS values. Figure 9 shows the same data for all targets considered in this study. For the stable targets in this mass range the default TALYS calculation produces MACS that are typically within a factor of two the recommended values. Also shown adjacent to the stable target MACS are error bars depicting the potential range of MACS from previous experiments and theory calculations. From these we see that factors of two (or more) from the recommended values have been quoted by previous experiments. Interestingly, all of the previous experiments quote uncertainties that are typically 5% or less.

We chose to normalize our default calculations to the recommended MACS by adjusting the TALYS parameter **gnorm**. Figure 10 shows the default values TALYS calculated and our adjustments, which were chosen to match the recommended MACS at 30 keV. We applied **gnorm** = 0.53 for all targets of Bi, 1.19 for $^{200-204}$Tl, and 2.83 for $^{205-207}$Tl. For Pb targets **gnorm** varied between 0.98 and 1.8.

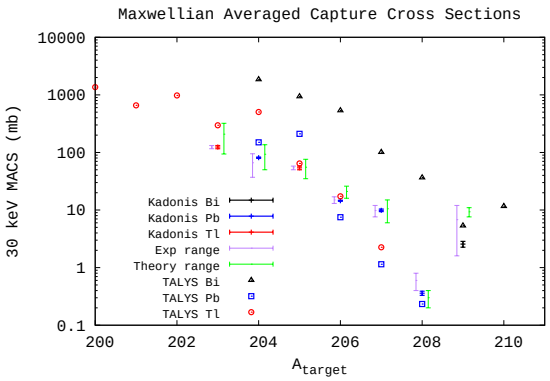

Fig. 9.— Maxwellian averaged capture cross sections (MACS) at 30 keV from KADONIS are shown vs. the default TALYS MACS values. Also shown adjacent to the experimentally determined MACS are error bars indicating the range of experimental and theory values cited by the KADONIS group in their evaluations.

Table 1: Default TALYS vs. 30 keV Maxwellian-averaged capture cross sections from KADONIS.

$^{A}Z_{target}$	KADONIS (mb)	TALYS (mb)	TAL/ KAD
^{209}Bi	2.56 ± 0.3	5.34	2.06
^{208}Pb	0.36 ± 0.03	0.23	0.64
^{207}Pb	9.90 ± 0.5	1.15	0.12
^{206}Pb	14.50 ± 0.3	7.52	0.52
^{204}Pb	81.00 ± 2.3	149.9	1.85
^{205}Tl	54.00 ± 4.0	64.4	1.19
^{203}Tl	124.00 ± 8.0	296.0	2.39

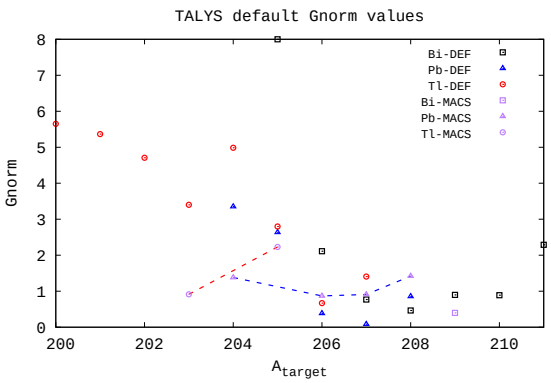

Fig. 10.— **Gnorm** values used by TALYS in default (red, blue, black shapes) and normalized (purple shapes) MACS calculations.

Figure 11 shows our Tl and Bi MACS calculated over the temperature range given by KADONIS. See Appendix B.3 for Pb MACS. The black dashed line shows the default TALYS calculation, the green solid line is our MACS with gnorm adjusted to agree at 30 keV. We chose the upper (red) and lower (blue) bounds according to the uncertainties on the average radiative widths for stable Tl and Bi targets. For all Tl targets we modified our adjusted gnorm value by ±20%. For all Bi targets we modified the normalized gnorm by ±30%. All normalized cross sections are plotted in Appendix C.

5. Conclusions

We have developed neutron induced cross sections for thallium ($Z = 81$, $200 \leq A \leq 207$), and bismuth ($Z = 83$, $204 \leq A \leq 210$) targets. The theory and implementation of the TALYS Hauser-Feshbach model was described (§2), as well as the default nuclear systematics that are constrained by experimental data (§3). Modeled cross sections were compared to available experimental cross sections for the loaded detector elements (Tl and Bi), as well as other stable targets in the region (Pb).

The TALYS default cross sections generally agree with experiment to within a factor of two for all reaction channels studied. We chose to adjust two parameters to bring the default calculations into agreement with the limited experimental cross section data in this region of interest: **M2constant** (used to normalize the (n,xn) cross sections) and **gnorm** (used to normalize the (n,γ) capture cross sections to evaluated MACS).

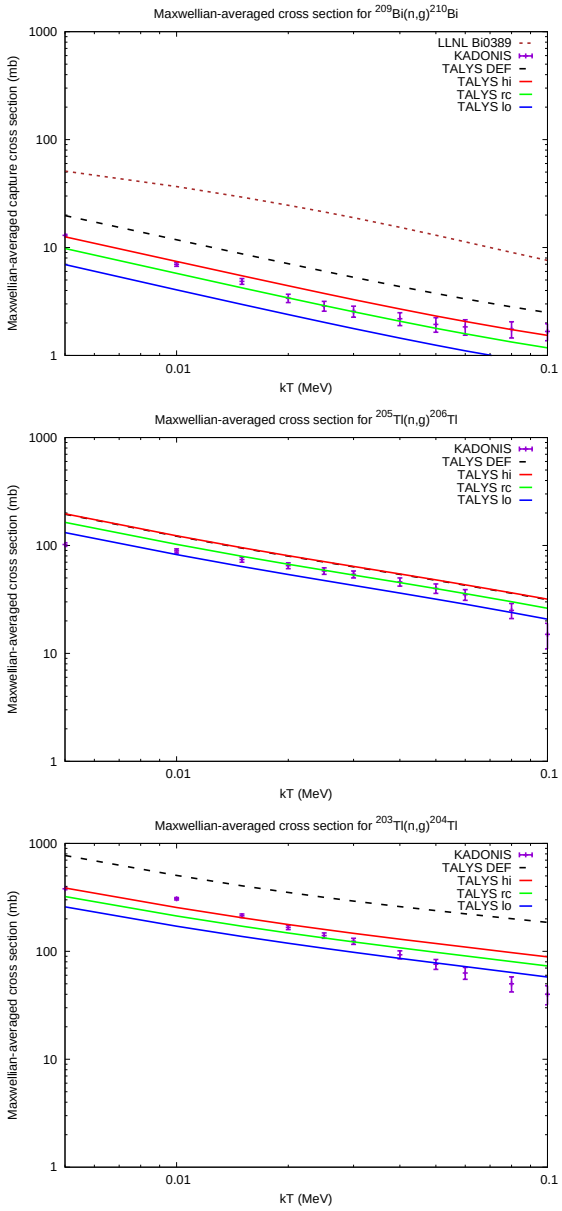

Fig. 11.— KADONIS Maxwellian averaged capture cross sections (MACS) and their uncertainties vs. TALYS. The black dashed line shows the TALYS default calculation, the three solid lines show the normalized calculation (green) and its upper(red) and lower(blue) bounds.

This work was performed under the auspices of the U.S. Department of Energy by the University of California Lawrence Livermore National Laboratory in part under contract W-7405-ENG-48 and in part under Contract DE-AC52-07NA27344.

REFERENCES

Audi, G., Wapstra, A.H., and Thibault, C., "The AME2003 atomic mass evaluation (II). Tables, graphs, and references", Nuc. Phys. A **729**, 337 (2003).

Bao, Z. Y., Beer, H., Kappeler, F., Voss, F., & Wisshak, K., "Neutron cross sections for nucleosynthesis studies", Atomic Data & Nuclear Data Tables, **76**, 70 (2000). See also Karlsrhue Astrophysical Database of nucleosynthesis in Stars (KADONIS) http://www.kadonis.org/

Beer, H., Voss, F., & Winters, R. R., "On the calculation of Maxwellian-averaged capture cross sections", ApJS, **80**, 403 (1992).

Belgya, T., Bersillon, O., Copote Noy, R., Fukahori, T., Zhigang, G., Goriely, S., Herman, M., Ignatyuk, A.V., Kailas, S., Koning, A.J., Oblozinsky, P., Plujko, V, and Young, P.G., "Handbook for calculations of nuclear reaction data, RIPL-2", IAEA, Vienna (2005).

Experimental Nuclear Reaction Data File, Brookhaven National Laboratory, US Dept. of Energy (2006). http://www.nndc.bnl.gov/exfor3/

Gilbert, A. and Cameron, A.G.W., "A composite nuclear-level density formula with shell corrections", Can. J. Phys., **43**, 1446 (1965).

Hauser, W. and Feshbach, H., "The inelastic scattering of neutrons", Phys. Rev. **87**, 366 (1952).

Hilaire, S., Lagrange, Ch., and Koning, A. J., "Comparisons between various width fluctuation correction factors for compound nucleus reactions" Ann. of Phys. **306**, 209 (2003).

Hoffman, R.D., Dietrich, F.S., Bauer, R., Kelley, K., and Mustafa, M.G., "Neutron and charged-particle induced cross sections for radiochemistry in the region of bromine and krypton", UCRL-TR-205563, LLNL (2004a).

Hoffman, R.D., Dietrich, F.S., Bauer, R., Kelley, K., and Mustafa, M.G., "Neutron and charged-particle induced cross sections for radiochemistry in the region of iodine and xenon", UCRL-TR-206721, LLNL (2004b).

Hoffman, R.D., Kelley, K., Dietrich, F.S., Bauer, R., and Mustafa, M.G., "Neutron and charged-particle induced cross sections for radiochemistry in the region of samarium, europium and gadolinium", UCRL-TR-211558, LLNL (2004c).

Hoffman, R.D., Kelley, K., Dietrich, F.S., Bauer, R., and Mustafa, M.G., "Modeled neutron and charged-particle induced nuclear reaction cross sections for radiochemistry in the region of yttrium, zirconium, niobium, and molybdenum", UCRL-TR-222275, LLNL (2006c)

Hoffman, R.D. "Modeled neutron and charged-particle induced nuclear reaction cross sections and their Uncertainties the Region $37 \leq Z \leq 47$ (Rb-Ag)", LLNL-TR-737934, LLNL, 2017

Hoffman, R.D., Dietrich, F.S., Kelley, K., Escher, J., Bauer, R., and Mustafa, M.G., "Modeled neutron and charged-particle induced nuclear reaction cross sections for radiochemistry in the region of iridium and gold", UCRL-TR-401969, LLNL (2008).

Hoffman, R.D. " Modeled Neutron Induced Nuclear Reaction Cross Sections for Radiochemistry in the region of Thulium, Lutetium and Tantalum I. Results of Built in Spherical Symmetry in a Deformed Region", LLNL-TR-643519, LLNL, 2015

Hofmann, H.M., Richert, J., Tepel, J. W., and Weidenmu̇ller, H.A., "Direct reactions and Hauser-Feshbach theory" Ann. of Phys. **90**, 403 (1975).

Iljinov, A.S., Mebel, M.V., Bianchi, N., De Sanctis, E., Guaraldo, C., Lucherini, V., Muccifora, V., Polli, E., Reolon, A.R., and Rossi, P., "Phenomenological statistical analysis of level densities, decay widths and lifetimes of excited nuclei", Nucl. Phys. A **543**, 517 (1992).

Kelley, K., Hoffman, R.D., Dietrich, F.S., Bauer, R., and Mustafa, M.G., "'Neutron and charged-particle induced cross sections for radiochemistry for isotopes of scandium, titanium, vanadium, chromium, manganese, and iron", UCRL-TR-211668, LLNL (2005).

Kelley, K., Hoffman, R.D., Dietrich, F.S., and Mustafa, M.G., "Neutron induced cross sections for radiochemistry for isotopes of arsenic", UCRL-TR-218181, LLNL (2006a).

Kelley, K., Hoffman, R.D., Dietrich, F.S., and Mustafa, M.G., "Neutron induced cross sections for radiochemistry for isotopes of nickel, copper, and zinc", UCRL-TR-221759, LLNL (2006b).

Koning, A.J., & Delaroche, J.P., "Local and global nucleon optical models from 1 keV to 200 MeV", Nucl. Phys. **A713**, 231 (2003).

Kopecky, J. and Uhl, M., "Test of gamma-ray strength functions in nuclear reaction model calculations", Phys. Rev. C **41**, 1941 (1990).

Mahaux, C. and Weidenmüller, H.A., "Recent developments in compound-nucleus theory", Ann. Rev. Part. Nucl. Sci. **29**, 1 (1979).

Moldauer, P. A., "Evaluation of the fluctuation enhancement factor" Phys. Rev. C **14**, 764 (1976).

Mughabghab, S.F., Divadeenam, M., and Holden, N.E., *Neutron Cross Sections*, Vols. 1 and 2, Academic Press (1981).

Nethaway, D.R., "The cross-section sets used with the Watusi program", A-Division memo, LLNL (5 Nov. 1998).

Raynal, J. "ECIS96", Proceedings of the Specialists' Meeting on the Nucleon Nucleus Optical Model up to 200 MeV, 13-15 November 1996, Bruyeres-le-Chatel, France. http://www.nea.fr/html/science/om200/raynal.pdf

Koning, A., Hilaire, S.,& Goriely, S. "TALYS-1.9: A nuclear reaction program", Dec. 28, 2011 http://www.talys.eu/

Wapstra, A.H., Audi, G., and Thibault, C., "The AME2003 atomic mass evaluation (I). Evaluation of input data, adjustment procedures", Nuc. Phys. A **729**, 129 (2003).

This 2-column preprint was prepared with the AAS LaTeX macros v5.0.

A. Input data included in the Detector Sets

Cross sections for (n,γ), (n,2n), and (n,3n) reactions on the target states listed below constitue the existing RADCHEM data set Bi0389. We will adopt the same target list for the new Bi set. The cross sections in the Bi0389 set were taken from the ACTL library (circa 1970, (Nethaway 1998)). A few were scaled to match measured cross sections at or around 14 MeV of incident neutron energy. The target list for Pb was chosen to compare calculated to measured cross sections.

A.1. Target states for Thallium, Lead, and Bismuth Detector Sets

^{A}Z	half-life	J^{π}	(n,γ)	(n,2n)	(n,3n)
^{200}Tl	26.10 h	2-	○	○	○
^{201}Tl	3.04 d	1/2+	○	○	○
^{202}Tl	12.31 d	2-	○	○	○
^{203}Tl	STABLE	1/2+	○	○	○
^{204}Tl	3.78 y	2-	○	○	○
^{205}Tl	STABLE	1/2+	○	○	○
^{206}Tl	4.20 m	0-	○	○	○
^{204}Pb	1.40×10^{17} y	0+	○	○	○
^{205}Pb	1.73×10^{7} y	5/2-	○	○	○
^{206}Pb	STABLE	0+	○	○	○
^{207}Pb	STABLE	1/2-	○	○	○
^{208}Pb	STABLE	0+	○	○	○
^{204}Bi	11.22 h	6+	○	○	○
^{205}Bi	15.31 d	9/2-	○	○	○
^{206}Bi	6.24 d	6+	○	○	○
^{207}Bi	31.55 y	9/2-	○	○	○
^{208}Bi	3.68×10^{5} y	5+	○	○	○
^{209}Bi	STABLE	9/2-	○	○	○
^{210}Bi	5.01 d	1-	○	○	○

A.2. Q-Values for Reactions Studied

Here we present the Q-values (in MeV) for each of the reactions included in this study. The values provided in this table are for reactions proceeding from the ground state of the target to the ground state of the residual. The values are calculated from our adopted mass excesses, as described in section 3.1.1.

Table 3:: Reaction Q-values

Target	$Q_{(n,\gamma)}$	$Q_{(n,2n)}$	$Q_{(n,3n)}$
^{200}Tl	8.205	-7.059	-15.661
^{201}Tl	6.780	-8.205	-15.264
^{202}Tl	7.852	-6.871	-15.076
^{203}Tl	6.656	-7.852	-14.723
^{204}Tl	7.546	-6.565	-14.509
^{205}Tl	6.504	-7.546	-14.202
^{206}Tl	6.852	-6.504	-14.050
Target	$Q_{(n,\gamma)}$	$Q_{(n,2n)}$	$Q_{(n,3n)}$
^{204}Pb	6.732	-8.395	-15.312
^{205}Pb	8.087	-6.732	-15.126
^{206}Pb	6.738	-8.087	-14.818
^{207}Pb	7.368	-6.738	-14.825
^{208}Pb	3.937	-7.368	-14.106
Target	$Q_{(n,\gamma)}$	$Q_{(n,2n)}$	$Q_{(n,3n)}$
^{204}Bi	8.490	-7.192	-16.047
^{205}Bi	7.035	-8.490	-15.682
^{206}Bi	8.098	-7.035	-15.525
^{207}Bi	6.887	-8.098	-15.133
^{208}Bi	7.460	-6.887	-14.985
^{209}Bi	4.605	-7.460	-14.347
^{210}Bi	5.138	-4.605	-12.064

A.3. Default TALYS Input file

```
#
# General parameters - Bi209 + n
#
projectile n
element    Bi
mass       209
energy     energies

# Assumed Models

# Level Density - BSFG + CTM - disc levels exp & theory to 100
ldmodel 1
disctable 1

# Gamma strength functions - EGLO
strength 1

# Gamma emmission
gammax 2
#gnorm 1.0

# Maxwell average (n,g) at 30 keV
#astroE 0.03

# Width Fluctuations - Moldauer
widthmode 1

# Pre-equillibrium - 2-component exciton model with analytical trans rates
preeqmode 1
twocomponent y
M2Constant 1.0

# Restriction on exit particles (no charged particles - very heavy targets)
ejectiles g n

# Ecis run parameters - set inncalc and eciscalc to "n" after first calculation
ecissave y
inccalc y
eciscalc y

# General parameters
best n

#
# Output
partable y
channels y
filechannels y
outgamma y
outdensity y
outomp n
```

Fig. 12.— TALYS input file for default Bi209 + n calculation

A.4. Level Density Parameters

Here we present the level density parameters, as described in section 3.3, for each target or compound nucleus considered in this study (column 1). The second through fifth columns are the fermi gas parameters: the asymptotic level density parameter $\tilde{a}$ (MeV^{-1}), the backshift Δ (MeV), the shell correction δW (MeV), and a flag that indicates whether $\tilde{a}$ is based on an experimentally measured resonance spacing (x) or is taken from systematics (s). The damping parameter (γ) for the shell correction was 0.0073. Next are the constant temperature fit parameters: the matching energy E_x where the fermi gas and constant temperature fits join, then the square of the spin cutoff parameter σ^2, the nuclear temperature T, and E_0 (both in MeV) all evaluated at E_x. The last three columns give the number of the excited states used in the contant temperature level density fit (starting at N_{low} and ending at N_{top}) and the average level spacing D_0 (keV) resulting from this choice of parameters.

Table 4: Level Density Parameters

Target	$\tilde{a}$	Δ	δW	x/s	E_x	$\sigma(E_x)^2$	T	E_0	N_{low}	N_{top}	D_0
^{200}Tl	23.522	0.000	-4.345	s	5.690	10.832	0.626	-1.717	2	30	0.025
^{201}Tl	23.623	0.846	-4.912	s	5.856	7.269	0.609	-0.422	3	15	0.011
^{202}Tl	23.725	0.000	-5.850	s	7.550	10.888	0.702	-1.992	2	30	0.098
^{203}Tl	23.826	0.842	-6.375	s	9.542	4.250	0.735	-1.350	7	17	0.046
^{204}Tl	24.487	0.000	-7.398	x	7.809	10.944	0.714	-1.396	8	26	0.280
^{205}Tl	24.029	0.838	-7.918	s	10.490	5.250	0.765	-0.780	5	18	0.216
^{206}Tl	22.239	0.000	-9.079	x	3.558	4.286	0.830	-0.314	2	15	5.500
^{207}Tl	24.231	0.834	-9.200	s	4.386	11.027	0.991	-0.803	2	30	9.761
^{208}Tl	24.332	0.000	-7.928	s	3.546	11.055	0.841	-1.617	2	10	5.539
^{204}Pb	23.927	1.680	-6.702	s	10.587	3.810	0.742	-0.422	2	17	0.072
^{205}Pb	24.897	0.838	-7.564	x	7.859	8.787	0.691	-0.269	8	17	2.000
^{206}Pb	24.130	1.672	-8.393	s	12.170	9.433	0.781	0.121	8	16	0.374
^{207}Pb	22.678	0.834	-9.554	x	1.830	12.472	0.621	1.608	3	15	2.000
^{208}Pb	21.507	1.664	-9.962	x	11.119	10.246	0.823	1.808	2	15	8.000
^{209}Pb	20.606	0.830	-8.608	s	6.285	12.463	0.754	0.920	2	33	2.717
^{204}Bi	23.927	0.000	-4.970	s	1.747	21.143	0.442	0.016	6	16	0.008
^{205}Bi	24.029	0.838	-5.660	s	6.273	14.560	0.631	-0.419	4	17	0.006
^{206}Bi	24.130	0.000	-6.586	s	4.057	15.253	0.600	-0.515	8	18	0.034
^{207}Bi	24.231	0.834	-7.191	s	8.494	10.609	0.713	-0.615	5	23	0.038
^{208}Bi	24.332	0.000	-8.265	s	5.953	14.722	0.687	-0.461	6	25	0.172
^{209}Bi	24.433	0.830	-8.532	s	1.532	10.488	0.565	1.264	5	15	0.293
^{210}Bi	22.520	0.000	-7.610	x	6.964	18.247	0.732	-0.904	8	21	4.000
^{211}Bi	24.635	0.826	-5.849	s	8.594	21.519	0.693	-1.342	6	22	1.502

B. Modeled Lead Cross Sections Compared to Experiment

B.1. Pb(n,2n) cross sections: TALYS vs. experiment

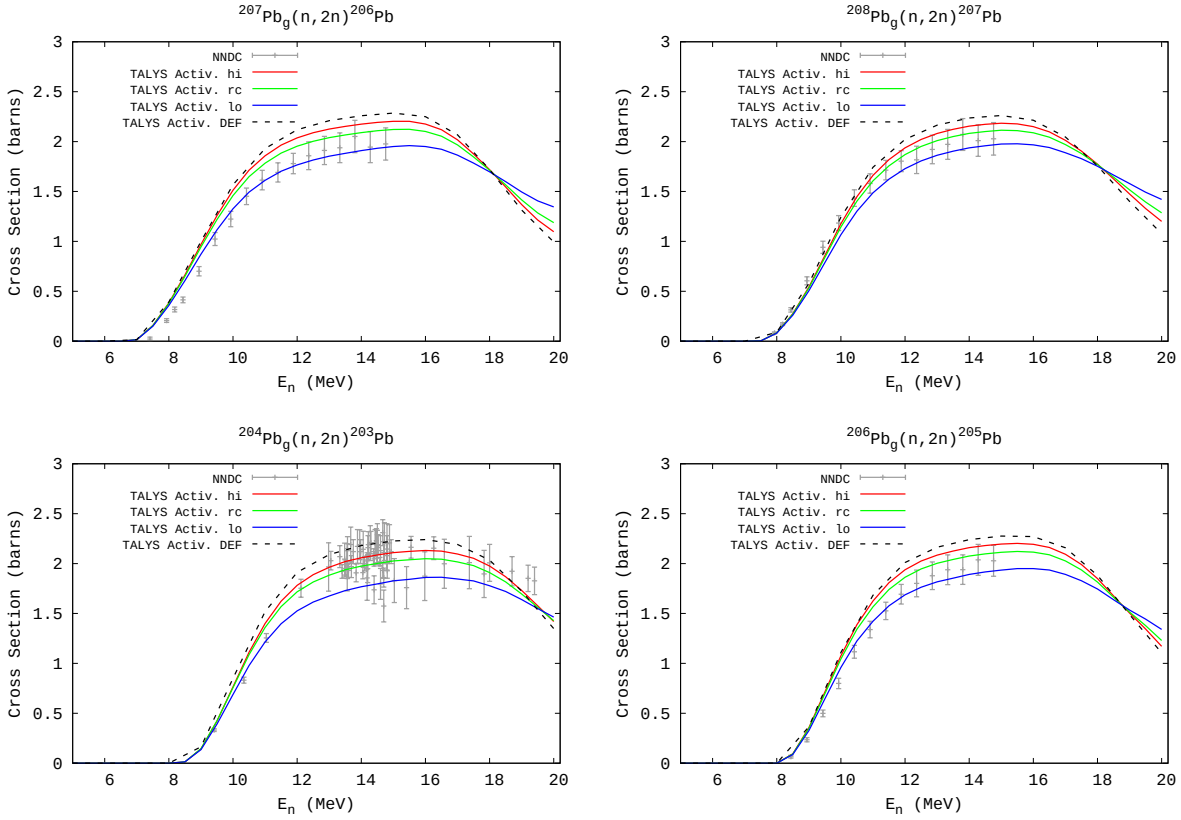

Fig. 13.— Modeled Pb(n,2n) cross sections compared to experiment (NNDC 2006).

B.2. Pb(n,3n) cross sections: TALYS vs. experiment

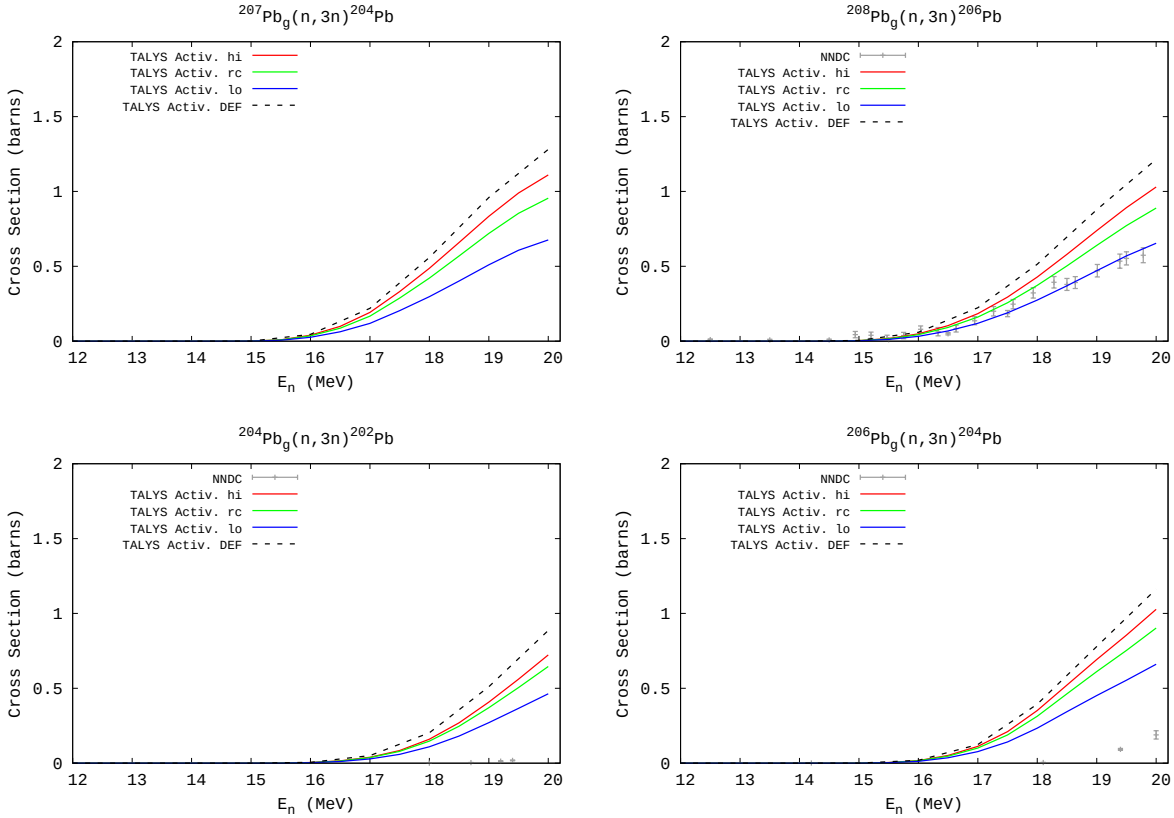

Fig. 14.— Modeled Pb(n,3n) cross sections compared to experiment (NNDC 2006). The experimental data for ^{204}Pb(n,3n)^{202m}Pb and ^{206}Pb(n,3n)^{204m}Pb represent the cross section going to the long lived (9-) isomer in each product nucleus, while the data for ^{208}Pb(n,3n)^{206g}Pb represents the cross section going to the ground state. The plotted TALYS results represent the total (n,3n) cross section.

B.3. Pb(n,γ) cross sections: TALYS vs. experiment

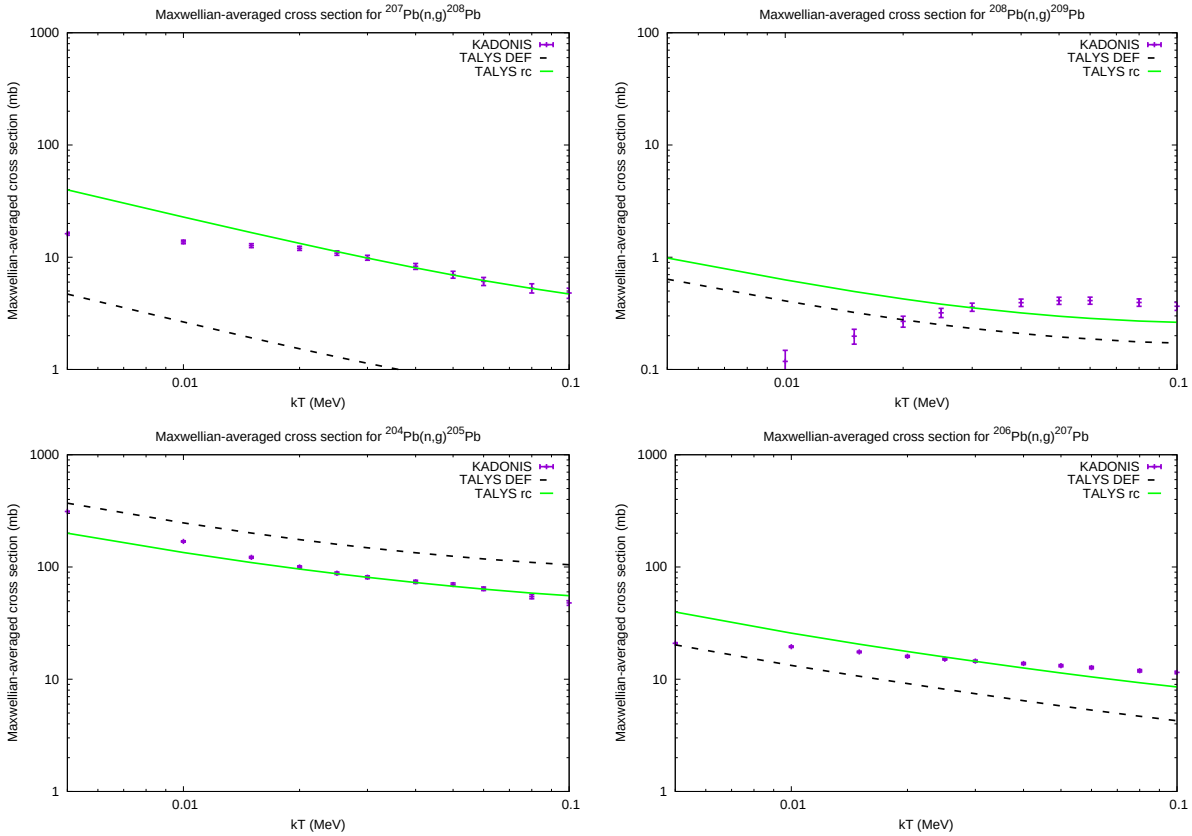

Fig. 15.— Maxwellian averaged capture cross sections (MACS) and their uncertainties for Pb targets from KADONIS vs. TALYS. The black dashed line shows the TALYS default calculation, the solid green line shows the normalized TALYS calculation.

C. Normalized Tl & Bi Cross Sections

C.1. Normalized (n,2n) cross sections

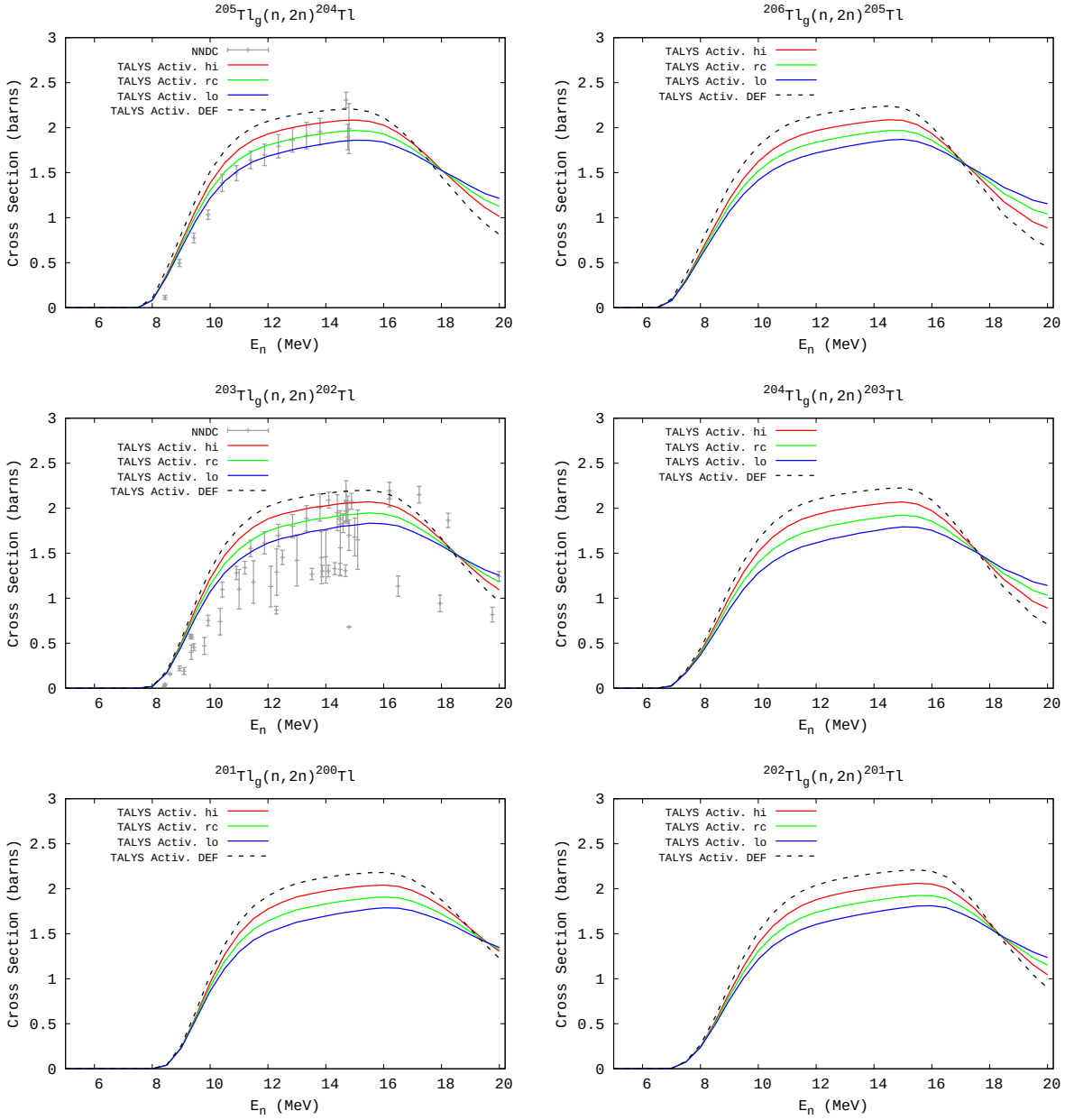

Fig. 16.— Normalized Tl(n,2n) cross sections

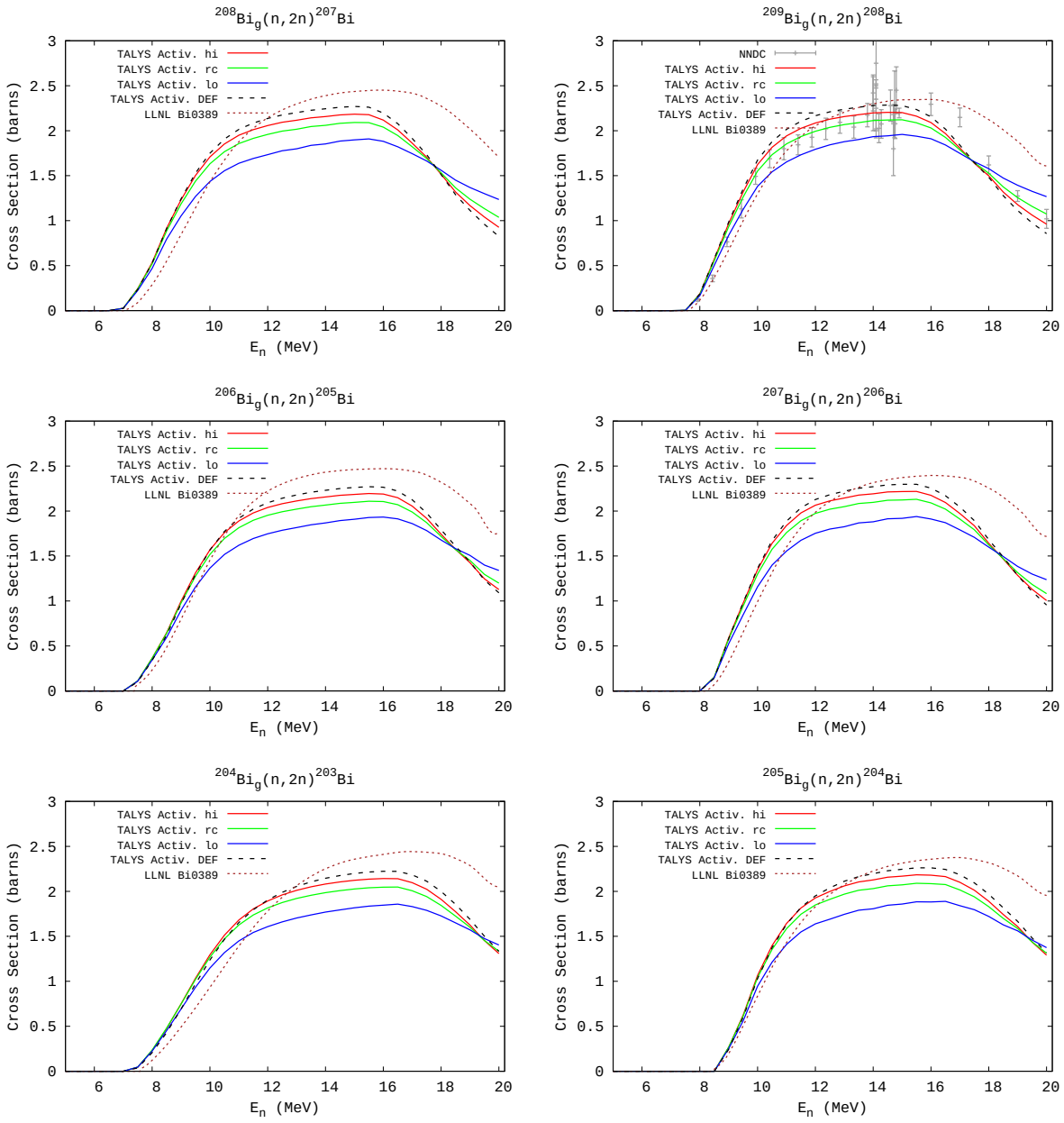

Fig. 17.— Normalized Bi(n,2n) cross sections

C.2. Normalized (n,3n) cross sections

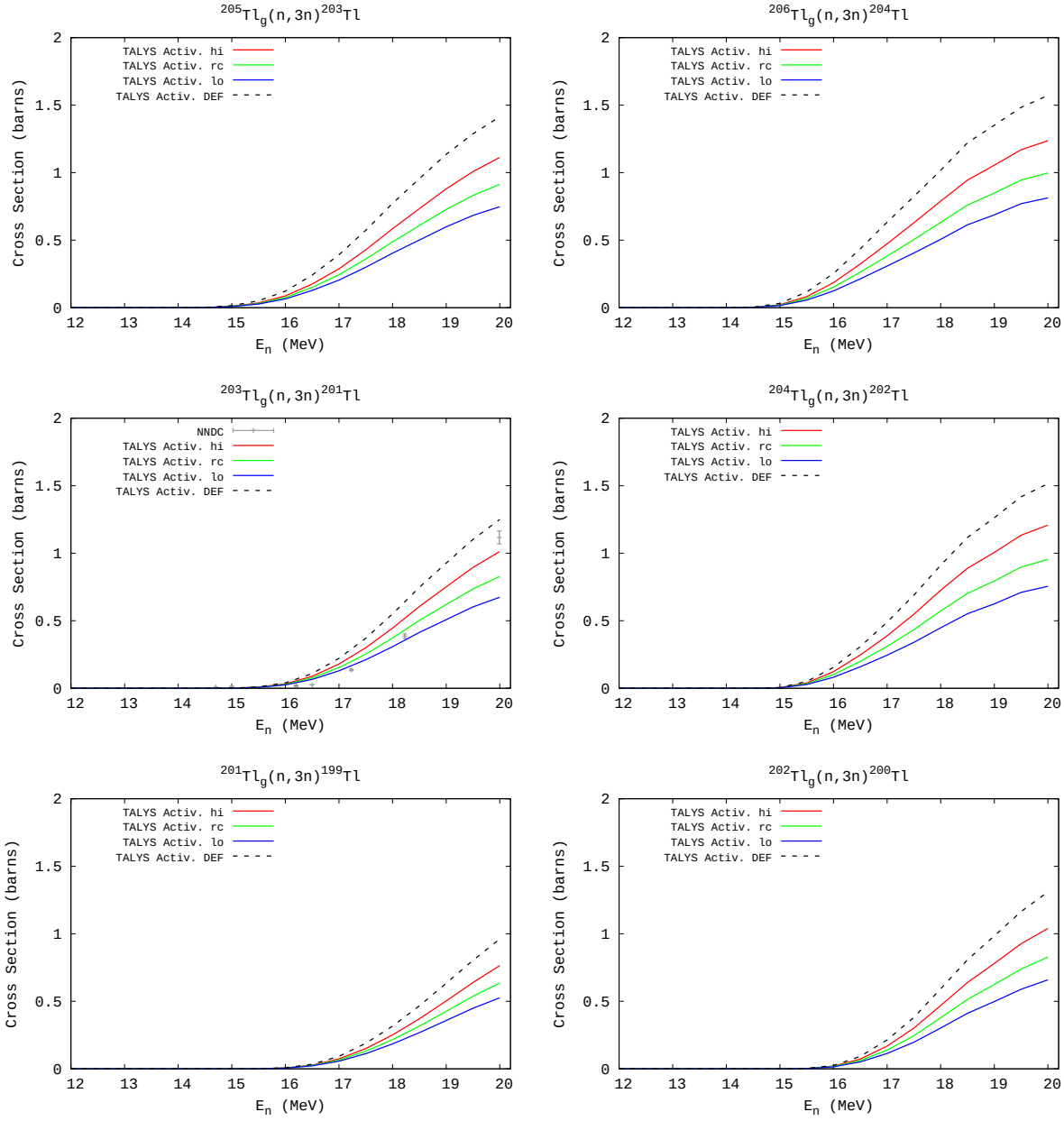

Fig. 18.— Normalized Tl(n,3n) cross sections

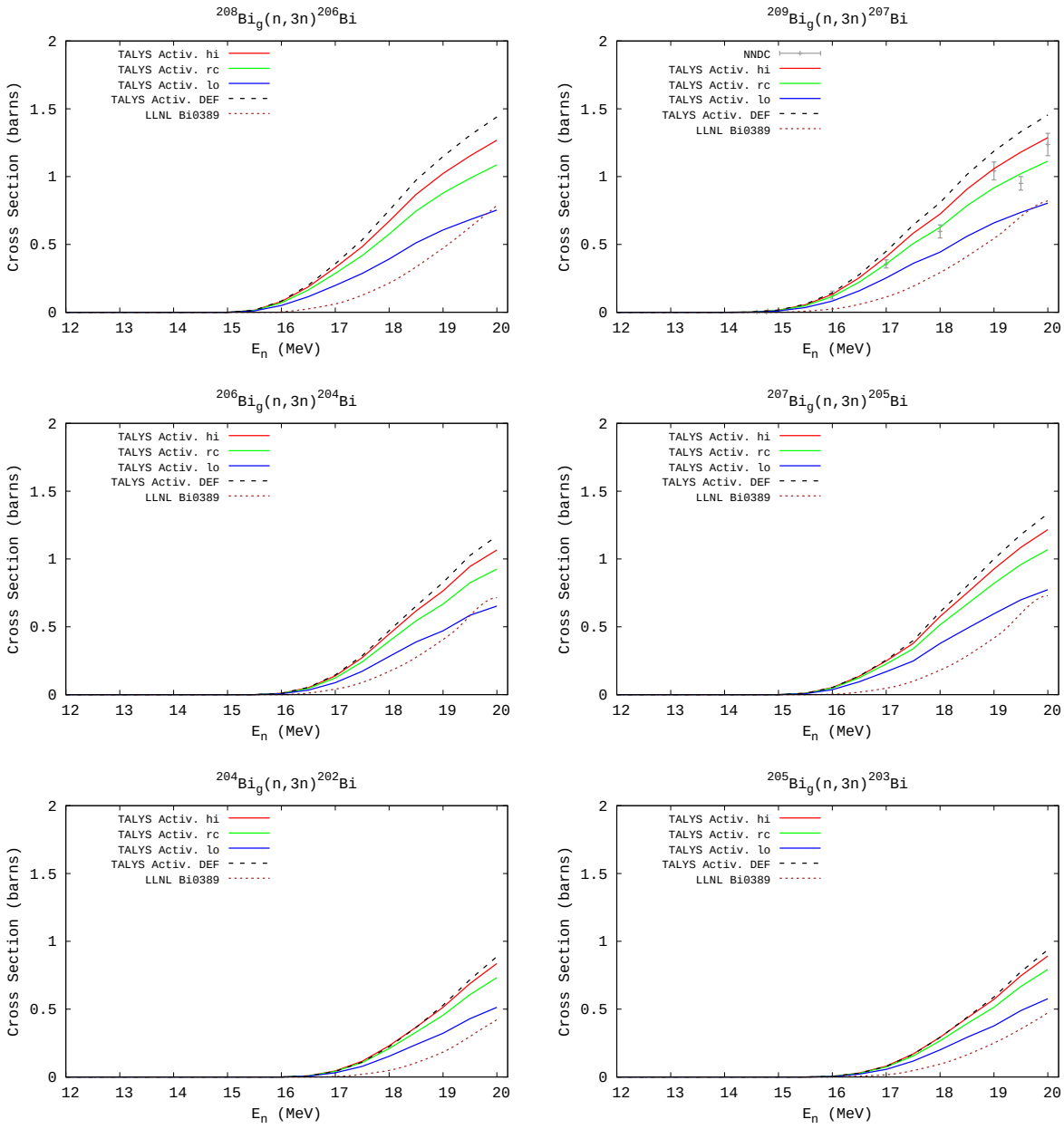

Fig. 19.— Normalized Bi(n,3n) cross sections

C.3. Normalized (n,γ) cross sections

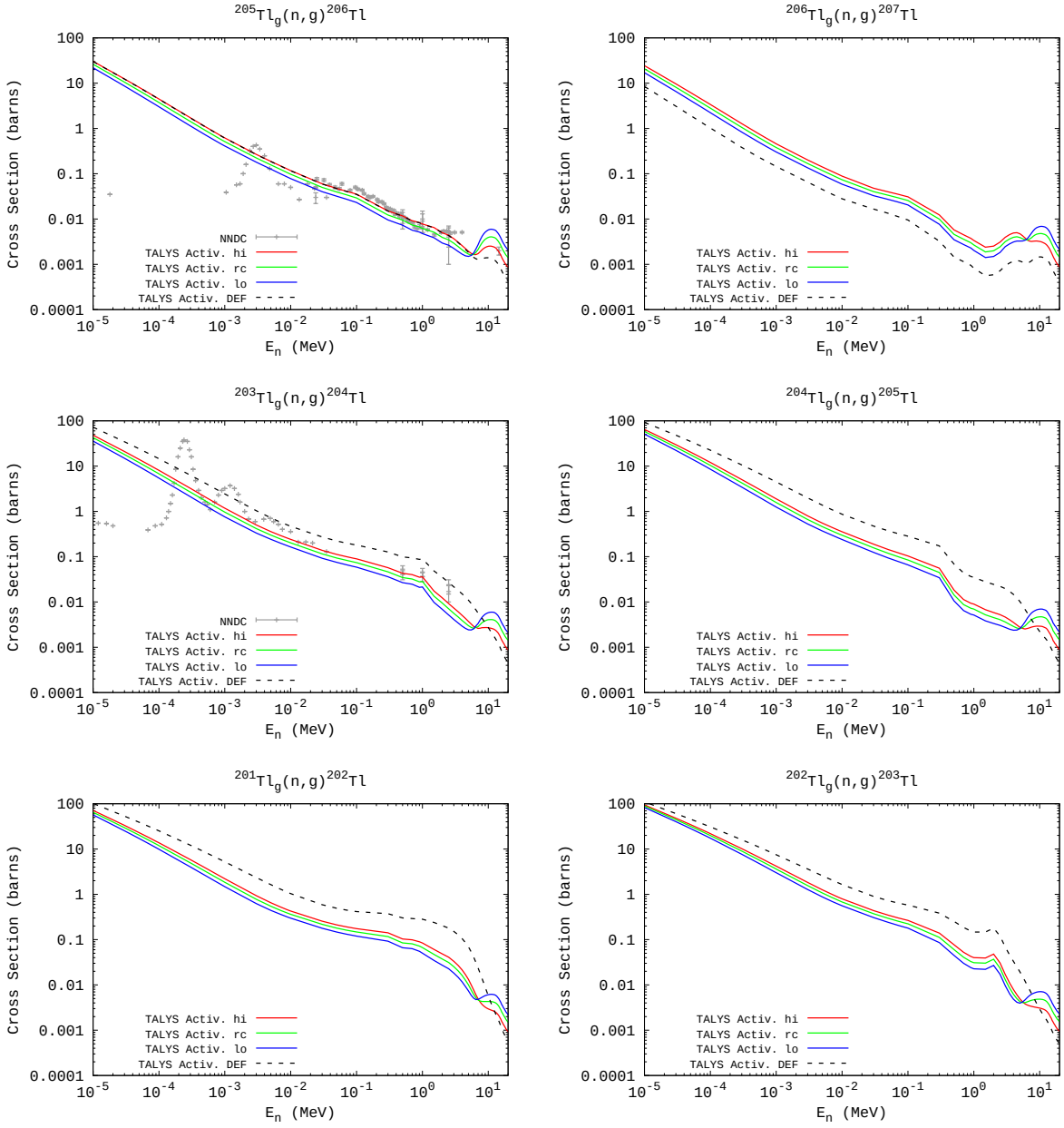

Fig. 20.— Normalized Tl(n,γ) cross sections

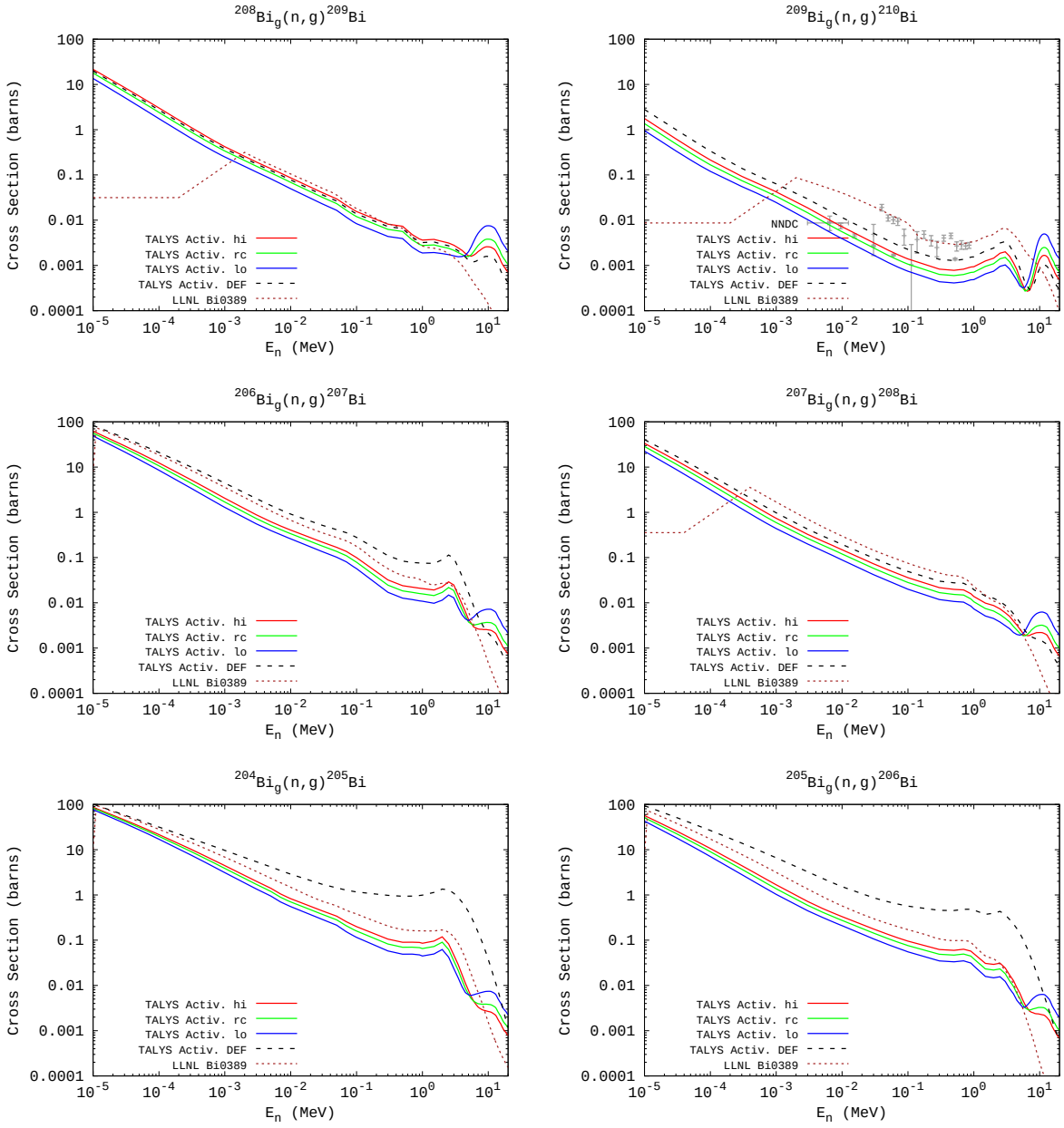

Fig. 21.— Normalized Bi(n,γ) cross sections